

# Current Challenges and Advanced Design Strategy of Vanadium Dioxide Cathode for Low-Cost Aqueous Zinc Metal Battery

Wenwei Zhang, Wenhui Zhong, Junjun Wang, Qinyou An,\* and Liqiang Mai\*


Rechargeable aqueous zinc metal battery has been one of the next-generation energy storage systems with a promising future due to the advantages of aqueous electrolyte and metallic zinc anode. Among many cathode materials, vanadium-based materials with considerable specific capacity, adjustable crystal structure, and multiple valence states are very promising cathodes, but the electrochemical performance of vanadium-based zinc metal batteries faces severe challenges such as the limited and declining capacity and sluggish ion/e<sup>-</sup> transport kinetics process. Herein, taking VO<sub>2</sub> as an example, the crystal structure and energy storage mechanism of VO<sub>2</sub> cathode are briefly introduced. The challenges of aqueous Zn/VO<sub>2</sub> battery are analyzed in depth. Significantly, the current advanced modification strategies for aqueous Zn/VO<sub>2</sub> battery are summarized and discussed in detail, and the future development is also prospected. This article can provide some significant references for the development of aqueous Zn/VO<sub>2</sub> battery and the guiding significance for other metal ion battery.

## 1. Introduction

Recently, aqueous zinc metal battery has received increasing attention due to the safe, low-cost, high ionic conductivity, and environmentally friendly water-based electrolyte.<sup>[1]</sup> Also, it can be attributed to the advantage of zinc anode, such as the low cost, high stability, suitable redox potential (−0.76 V vs standard hydrogen electrode (SHE)), considerable specific capacity (820 mA h g<sup>-1</sup> and 5855 mA h cm<sup>-3</sup>), and 2 e<sup>-</sup> transfer.<sup>[2]</sup>

W. Zhang, J. Wang, Q. An, L. Mai  
State Key Laboratory of Advanced Technology for Materials Synthesis and Processing  
Wuhan University of Technology  
Wuhan 430070, China  
E-mail: anqinyou86@whut.edu.cn; mlq518@whut.edu.cn

W. Zhong  
School of Materials and Chemical Engineering  
Hubei University of Technology  
Wuhan 430068, China

 The ORCID identification number(s) for the author(s) of this article can be found under <https://doi.org/10.1002/aesr.202300139>.

© 2023 The Authors. Advanced Energy and Sustainability Research published by Wiley-VCH GmbH. This is an open access article under the terms of the Creative Commons Attribution License, which permits use, distribution and reproduction in any medium, provided the original work is properly cited.

DOI: 10.1002/aesr.202300139

Regrettably, the further application and exploration of cathode materials are prevented by the strong electrostatic force between the cathode material and Zn<sup>2+</sup> ions with high charge density, and also the dissolution of elements in the main material, which all can damage the structure and lead to material failure.<sup>[3]</sup> Therefore, designing and developing a practical cathode material with a stable structure, fast transfer kinetics, and considerable power/energy density is significant and necessary for aqueous zinc metal battery (AZMB).

The significant cathode systems mainly include manganese-, vanadium-, organic-, Prussian blue-based materials, and others.<sup>[3a,b]</sup> Among them, the Jahn–Teller effect of manganese element, and the complex and controversial energy storage

mechanism in manganese-based cathodes has become the major challenges for AZMB, such as the limited cycle life.<sup>[4]</sup> And, the limited specific capacity caused by the underutilized reactive sites also is not conducive to the development and application of Prussian blue-based materials.<sup>[5]</sup> Additionally, the products of organic cathode materials after the discharge process will be slightly soluble in water-based electrolytes, and side reactions may occur on the surface of the zinc anode, which will lead to a decrease in capacity.<sup>[6]</sup> Compared to the above common cathode materials, the vanadium-based materials have gained the favor of researchers due to the relatively stable and varied structure, promising zinc ion storage ability, etc. Typically, VO<sub>2</sub>, one of the most popular vanadium-based materials in energy storage, has been considered as a significant potential cathode due to the applicable specific capacity, suitable structure, and large lattice spacing for the Zn<sup>2+</sup> ion insertion/extraction.<sup>[7]</sup> However, the slow transfer kinetics and relative low specific capacity were mainly caused by the disadvantages of structural collapse, poor conductivity, and vanadium dissolution, which will hinder further practical application in the future. Also, the discharge voltage plateau is not sufficient for sufficient energy/power density when compared with the existing manganese- and Prussian blue-based materials.

Interestingly, the increasing number of research about VO<sub>2</sub>-based cathode materials has been reported well for AZMB, especially the development of a modification strategy on the embarrassing issues of Zn/VO<sub>2</sub> battery. However, to the best of our knowledge, there are no specific reviews focused on the VO<sub>2</sub>-based cathode for AZMB, although the basic and

comprehensive reviews on the recent development of cathode materials (especially vanadium-based cathode) for AZMB have been concluded based on the bright application prospect for the energy storage. Usually, the reviews always focus on the whole development of AZMB or a specific cathode system (such as manganese-, vanadium-based materials, etc.).<sup>[3a,b,8]</sup> However, those reviews always only have small sections about the vanadium-based cathode, especially for a particular class of materials such as VO<sub>2</sub>.

Therefore, in this case, the systematic review of the structure, storage mechanism, challenges, and modification strategy in detail including the considerable and promising prospects of VO<sub>2</sub>-Zn battery is of great significance and necessity based on the above discussion.

In this article, we first introduced the crystal structure of VO<sub>2</sub> cathode and the corresponding Zn<sup>2+</sup> ion storage mechanism of an aqueous VO<sub>2</sub>//Zn battery (AVZB). Then, the challenges of AVZB have been concluded and analyzed in detail. Also, the advanced modification strategies for the storage of Zn<sup>2+</sup> ions of VO<sub>2</sub> are analyzed and discussed in detail. Finally, the development prospects of VO<sub>2</sub>-based cathode materials are conducted from a valuable point of view. This current review will produce significant guidance to the application of VO<sub>2</sub>-based materials for AZMB and modification strategy for rechargeable metal-ion batteries.

## 2. Crystal Structure and Zn<sup>2+</sup> Ion Storage Mechanism of VO<sub>2</sub>

### 2.1. Crystal Structure

The crystal structure of VO<sub>2</sub> will be transformed as the temperature changes and this phase change temperature is 68 °C, which

leads to many kinds of VO<sub>2</sub> crystal forms in nature. There are mainly tetragonal VO<sub>2</sub>(A), monoclinic VO<sub>2</sub>(M), VO<sub>2</sub>(D), and VO<sub>2</sub>(B), tetragonal rutile VO<sub>2</sub>(R), and triclinic VO<sub>2</sub>(T),<sup>[9]</sup> which can have mutual transformation between them under certain conditions. Presently, a variety of vanadium dioxide polymorphs (A-, B-, D-, and M-VO<sub>2</sub>) have been demonstrated to act as cathode materials for AZMB and deliverability of Zn<sup>2+</sup> ions storage.<sup>[7b,10]</sup>

As shown in **Figure 1a**, the VO<sub>2</sub>(A) belongs to the P42/ncm space group, and the V<sup>4+</sup> ion bonding with the 6 O<sup>2-</sup> ions and V–O bond distances ranges from 1.70 to 2.29 Å. And, the first different O<sup>2-</sup> ion has chemical bonds with four equivalent V<sup>4+</sup> ions while the second O<sup>2-</sup> ion could lead to linear geometry to two equivalent V<sup>4+</sup> atoms. And, the largest size of the tunnel is 3.64 × 3.64 Å which can accommodate the Zn<sup>2+</sup> ion with a radius of 0.76 Å.

Then, VO<sub>2</sub>(B) belongs to the monoclinic C2/m space group and exists two in equivalent V<sup>4+</sup> sites (Figure 1b). The first one bonded six-coordinate O<sup>2-</sup> ions with the V–O bond distances of 1.68–2.31 Å. While the other one bonded to six O<sup>2-</sup> ions with the edge and corner-sharing VO<sub>6</sub> octahedral, where the V–O bond distances can range from 1.83 to 2.10 Å and the tilt angles of 25°. As the O<sup>2-</sup> ion, the first O<sup>2-</sup> ion site bonded to two V<sup>4+</sup> ions, the second O<sup>2-</sup> ion site bonded to four V<sup>4+</sup> ions to produce OV<sub>4</sub> trigonal pyramids by the coexisting of distorted edge and corner-sharing. The third one is bonded in a distorted trigonal non-coplanar geometry to three V<sup>4+</sup> ions. And the last one is bonded in a distorted T-shaped geometry to three V<sup>4+</sup> ions. Usually, it shows the largest size of the tunnel (4.18 and 3.59 Å) for the Zn<sup>2+</sup> ion insertion/extraction process.

As the VO<sub>2</sub>(D) crystal structure (Figure 1c), it shows the zigzag chain-like network, which was built from one chain including distorted [V(1)O<sub>6</sub>] octahedral with alternating edge-sharing

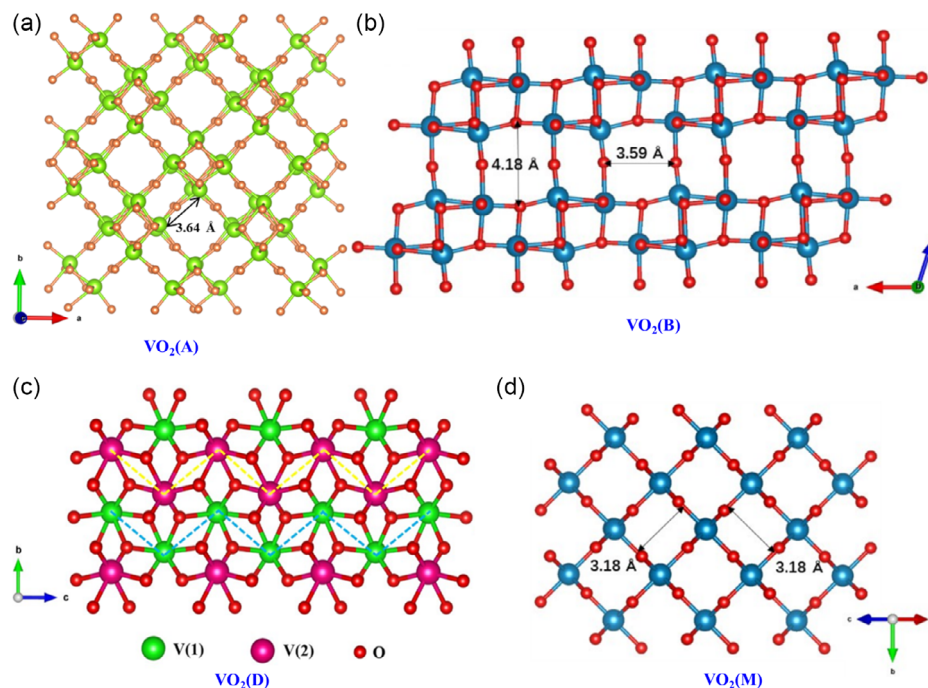


**Figure 1.** The crystal structure of VO<sub>2</sub> has been applied in aqueous zinc metal battery. a) VO<sub>2</sub>(A). b) VO<sub>2</sub>(B).<sup>[23]</sup> c) VO<sub>2</sub>(D).<sup>[11]</sup> d) VO<sub>2</sub>(M).<sup>[23]</sup> (b–d) Reproduced with permission.<sup>[11,23]</sup> Copyright 2019, The Royal Society of Chemistry.

and then linked to another [V(2)O<sub>6</sub>] octahedra under the connection of corner-shared O<sup>2-</sup> ions.<sup>[11,12]</sup> Moreover, when the temperature is higher than the phase transition temperature of 68 °C, the VO<sub>2</sub>(R) phase is transformed into VO<sub>2</sub>(M), and the V<sup>4+</sup> at the apex of the cell is shifted, resulting in the dimerization of the V-V chain in the direction of the C<sub>R</sub> axis, forming a long and short zigzag chain, in which the long bond is 3.19 Å and the short bond is 2.60 Å. The VO<sub>6</sub> octahedron also changes from a regular octahedron to a twisted octahedron (Figure 1d).

However, the VO<sub>2</sub> with different crystal from the above discussion will induce the diversified diffusion pathway for Zn<sup>2+</sup> ion insertion/extraction, thus the above VO<sub>2</sub> usually deliver differentiated electrochemical properties. In conclusion, the VO<sub>2</sub>(B) has the most suitable tunnel size to achieve a reversible Zn<sup>2+</sup> ion inserting/extracting process and received the most attention. Thus, the following part will mainly take VO<sub>2</sub>(B) as an example to summarize and discuss in detail.

## 2.2. Energy Storage Mechanism

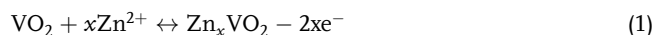
Usually, the metal anode will become the corresponding metal ions and move to the cathode material under the action of electrolyte during the discharge process in rechargeable metal battery, while the opposite reaction process occurs during the subsequent charging process in principle. Currently, two different reaction mechanisms are believed to exist simultaneously in this process with the continuous exploration of energy storage mechanisms for rechargeable metal-ion batteries, including

AVZB.<sup>[13]</sup> Moreover, the types of charge ions involved in the reaction have also been demonstrated to be not only Zn<sup>2+</sup> ions. On the one hand, the charge ion will be inserted into the cathode for the redox reaction; On the other hand, the pseudo-capacitive Faradaic process occurs near the surface via the electric double layer capacitors effect.

### 2.2.1. Diffusion-Controlled Faradaic Process

*The Single Ion Insertion/Extraction Mechanism:* Under this mechanism, the Zn<sup>2+</sup> ions move to VO<sub>2</sub> via the electrolyte during the discharge process and undergo the Faraday diffusion process, while the metal Zn anode is oxidized to Zn<sup>2+</sup> ion (Equation (1)–(3)). The reversible and opposite process will occur at the charge process. In this process, the Zn<sup>2+</sup> ion will cause the lattice changes, such as increasing or decreasing the layer spacing. Chen et al. demonstrated this highly reversible single-phase reaction under the conduction of in situ X-ray diffraction (XRD) technology.<sup>[7a]</sup> The amount of Zn<sup>2+</sup> ion insertion into VO<sub>2</sub> and the corresponding structural changes were analyzed. Currently, this single Zn<sup>2+</sup> ion storage mechanism of VO<sub>2</sub> electrode has been accepted and found in most AVZB (Figure 2a).

Cathode



Anode

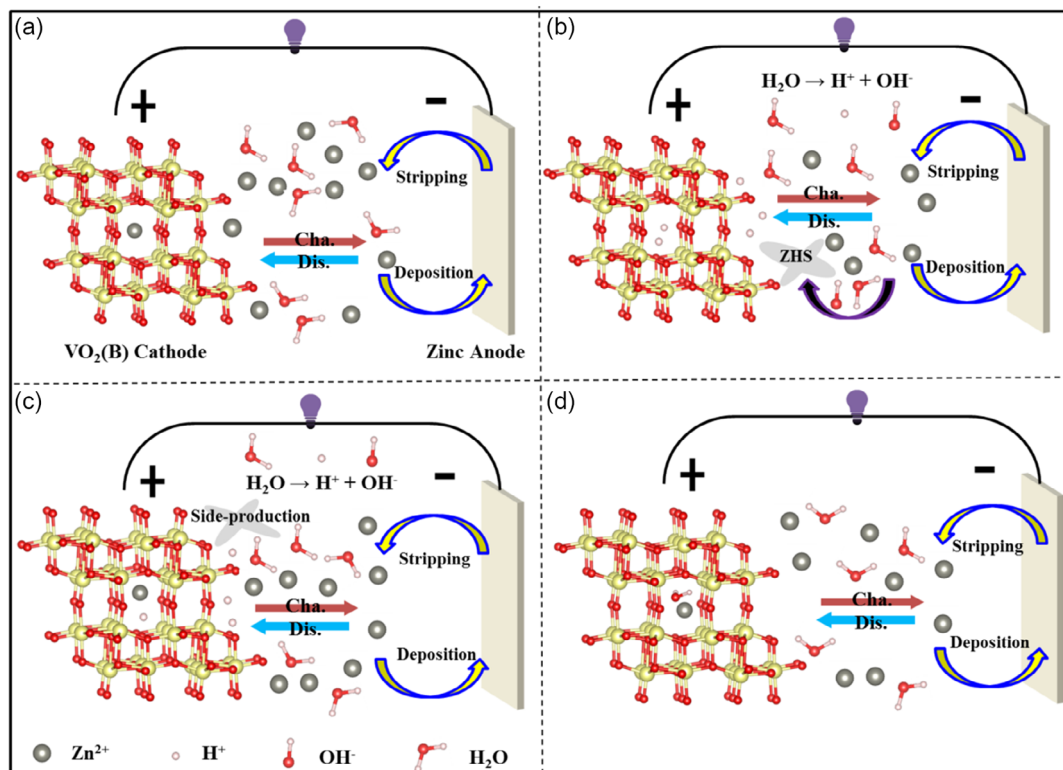


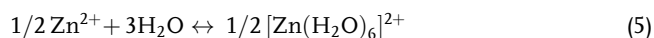
**Figure 2.** The diffusion-controlled storage process in AVZB (the structure diagram takes VO<sub>2</sub>(B) as a typical example). a) Zn<sup>2+</sup> ions. b) H<sup>+</sup> ions. c) Coininsertion of Zn<sup>2+</sup> ions and H<sup>+</sup> ions. d) Coininsertion of Zn<sup>2+</sup> ions and H<sub>2</sub>O.

Overall

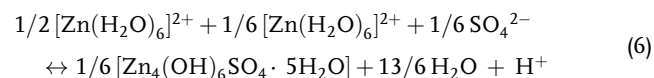


Usually, the  $\text{Zn}^{2+}$  ions are considered as only charge ions to insert/extract into/from the  $\text{VO}_2$  cathode in AVZB. However, the proton also has been found to be inserted into the  $\text{VO}_2$ -based cathode material.<sup>[14]</sup> In this case, the  $\text{H}^+$  ions with a smaller radius and one positive charge than the hydrated zinc ions would greatly enhance ion migration kinetics and maintain structural stability well by reducing the electrostatic force with the host material (Figure 2b). Li et al. demonstrated one new reaction mechanism that proton originating from the  $\text{H}_2\text{O}$  molecules can insert into  $\text{VO}_2$  and the  $\text{Zn}^{2+}$  ion reacted with electrolyte to deposit the  $\text{Zn}_4(\text{OH})_6\text{SO}_4 \cdot 5\text{H}_2\text{O}$  at the  $\text{VO}_2$  surface to store  $\text{Zn}^{2+}$  ion during the discharge process (Equation (4)–(8)) under the combination of theoretical calculation simulations and in/ex situ characterization (such as XRD, X-ray photoelectron spectroscopy (XPS), and neutron activation analysis (NAA)).<sup>[15]</sup> Also, they concluded that the proton insertion will rely on the anion with different solvation energy (such as large  $\text{CF}_3\text{SO}_3^-$  and small  $\text{SO}_4^{2-}$ ) proton insertion energetics.

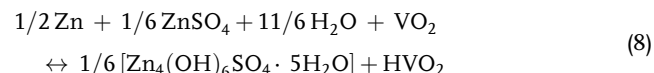
Anode



Cathode

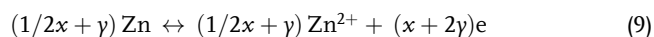


Overall

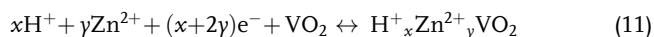


*The Dual Ion Coinsertion/Extraction Mechanism:* In recent years, the proton has been found to be inserted into the  $\text{VO}_2$  cathode material along with  $\text{Zn}^{2+}$  ions with the in-depth characterization of the energy storage mechanism for AVZB (Figure 2c). This  $\text{H}^+/\text{Zn}^{2+}$  hydrated ion insertion mechanism can not only effectively provide higher specific capacity from extra  $\text{H}^+$  ion, but also accelerate the reaction transport kinetics due to the smaller ionic radius and less positive charge of hydrogen ions. The  $\text{H}^+$  ion always preferentially inserts into  $\text{VO}_2$  at the higher voltage range and the  $\text{H}^+/\text{Zn}^{2+}$  coinsertion at the lower voltage range. This reaction process can be presented as follows:

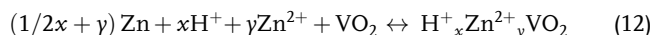
Anode



Cathode



Overall



In addition, the remaining hydroxide ions will react with the anion/cation ( $\text{Zn}^{2+}$ ,  $\text{SO}_4^{2-}$ ,  $\text{CF}_3\text{SO}_3^-$ , and  $\text{TFSI}^-$ , etc.) in the electrolyte to produce by-products, such as  $\text{Zn}(\text{OH})_2$ . In this case, the electrolyte may be consumed and not conducive to long-term cycling life as well as the side products on the surface of  $\text{VO}_2$  could increase the transport resistance of  $\text{Zn}^{2+}$  ions.

Additionally, the coinsertion of  $\text{Zn}^{2+}$  and hydrated zinc ions of  $[\text{Zn}(\text{H}_2\text{O})_6]^{2+}$  or  $\text{Zn}^{2+}$  and pure  $\text{H}_2\text{O}$  can occur on the extended structure and the  $\text{H}_2\text{O}$  can play the role in shielding part of the strong electrostatic force between  $\text{Zn}^{2+}$  ion and host materials of  $\text{VO}_2$  (Figure 2d).<sup>[16]</sup>

*The Chemical Phase Transition Mechanism:* In general, the vanadium element in  $\text{VO}_2$  is an intermediate valence state of +4, which first will lead to be converted to a more stable vanadium oxide-based material with high valence of +5 for higher specific capacity under specific cycling conditions. And, this new phase acts as the subsequent host material to store charge ion. Recently, Deng et al.<sup>[17]</sup> found that the argon-treated  $\text{VO}_2$  can induce self-phase transformation into  $\text{V}_2\text{O}_5 \cdot n\text{H}_2\text{O}$  as new cathode material at the initial charge process by the electrochemical oxidation and water insertion (Figure 3a). This resulting  $\text{V}_2\text{O}_5 \cdot n\text{H}_2\text{O}$  has higher theoretical specific capacity and a self-adaptive layer transformation structure connected by van der Waals forces for the enhanced significantly specific capacity and cycle stability. Similarly, Deng et al., Chen et al., and Li et al. also found this phase transformation from the initial  $\text{VO}_2$  into  $\text{V}_2\text{O}_5 \cdot n\text{H}_2\text{O}$  delivers outstanding performance.<sup>[11,17,18]</sup> Moreover, this phase transition product may also be zinc vanadate compounds (such as  $\text{Zn}_3(\text{OH})_2\text{V}_2\text{O}_7 \cdot 2\text{H}_2\text{O}$ ,  $\text{Zn}_2\text{V}_2\text{O}_7$  and  $\text{Zn}_{0.25}\text{V}_2\text{O}_5 \cdot n\text{H}_2\text{O}$ , Figure 3b–d) as cathode material to storage charge ions for AZMB with superior performance based on the  $\text{VO}_2$  and inserted zinc ions reacting with the electrolyte during the initial cycling process.<sup>[19]</sup>

However, the detailed transformation mechanism of this phase transition reaction needs further detailed discussion, such as the transition condition. In addition, it is accurate to calculate the specific capacity and diffusion kinetics according to the relevant parameters before the transformation after the transformation of  $\text{VO}_2$  into a new phase?

### 2.2.2. Pseudocapacitor-Controlled $\text{Zn}^{2+}$ Ion Storage Process

Pseudocapacitor processes of Faraday redox reactions that occur near or on the surface of  $\text{VO}_2$  cathode material, which could be beneficial to achieve high power and energy density for AVZB based on the significant improvement of sluggish solid-state diffusion of  $\text{Zn}^{2+}$  ions within the  $\text{VO}_2$ . Notably, this pseudocapacitive process, which is only on a timescale comparable to that of electric double-layer capacitors, still belongs to the redox reaction of battery-type storage in principle (Figure 4).<sup>[13]</sup> Usually, it mainly includes the intercalation pseudocapacitive process without phase transitions and the surface redox pseudocapacitance process.<sup>[20]</sup> And, the significant difference of the above typical pseudocapacitive storage process is that it is not affected by the slow reaction kinetics of solid diffusion.<sup>[13,20,21]</sup>

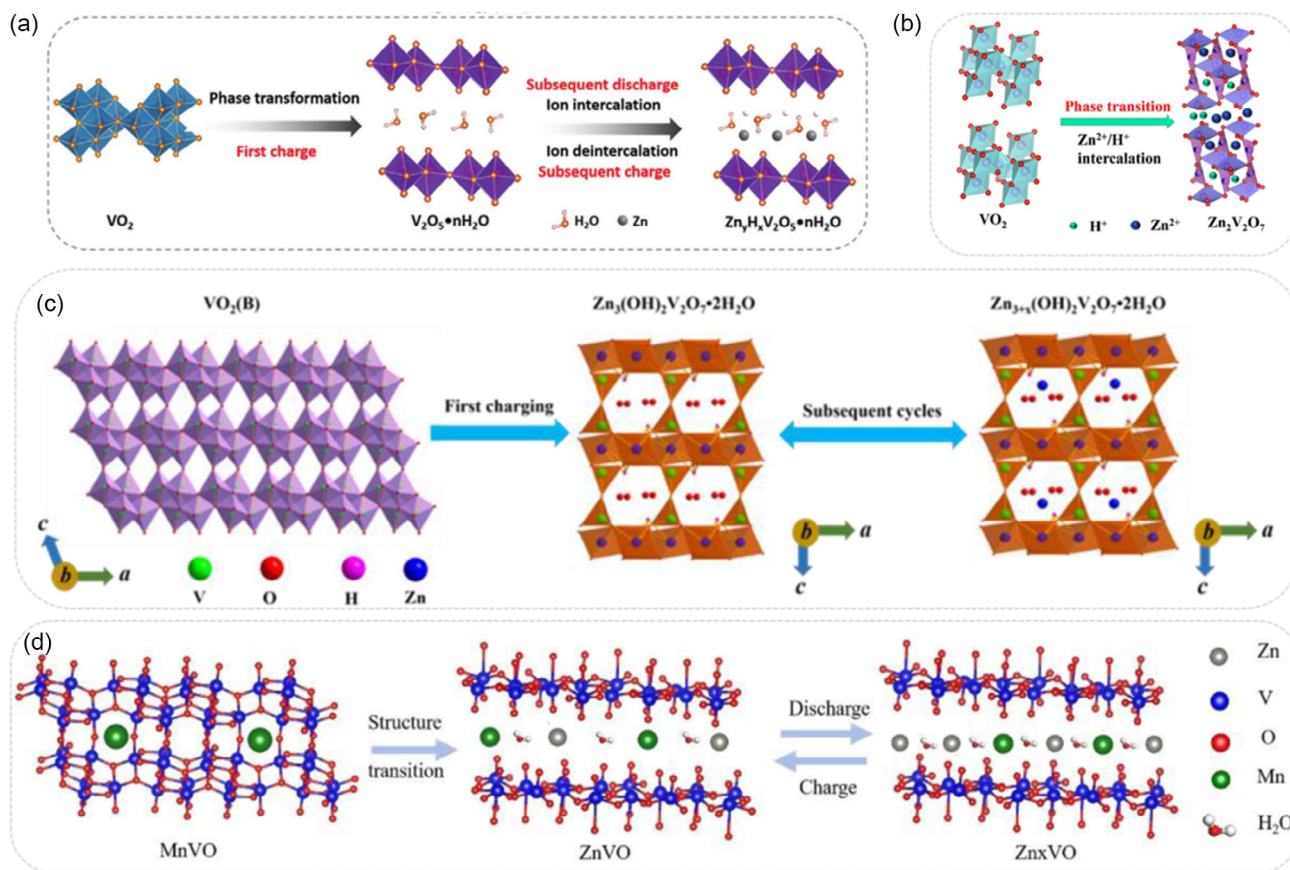


**Figure 3.** The chemical phase transition mechanism in AVZB. a) V<sub>2</sub>O<sub>5</sub>·nH<sub>2</sub>O. Reproduced with permission.<sup>[17]</sup> Copyright 2023, Wiley-VCH. b) Zn<sub>2</sub>V<sub>2</sub>O<sub>7</sub>. Reproduced with permission.<sup>[19b]</sup> Copyright 2023, Elsevier. c) Zn<sub>3</sub>(OH)<sub>2</sub>V<sub>2</sub>O<sub>7</sub>·2H<sub>2</sub>O. Reproduced with permission.<sup>[19c]</sup> Copyright 2021, Elsevier. d) Zn<sub>0.25</sub>V<sub>2</sub>O<sub>5</sub>·nH<sub>2</sub>O. Reproduced with permission.<sup>[19a]</sup> Copyright 2023, Elsevier.

Therefore, the proportion of the pseudocapacitor-controlled Zn<sup>2+</sup> ion storage process will increase significantly after improving the ion/electron transport kinetics, such as the reconstruction of crystal and electronic structures, or designed specific microstructure, etc.

Liu et al.<sup>[22]</sup> recently prepared VO<sub>2</sub>·xH<sub>2</sub>O with crystal water molecules and defects as cathodes for AVZB and demonstrated the reaction mechanism of intercalation pseudocapacitive Zn<sup>2+</sup> storage. Benefitting from this structure and mechanism, the VO<sub>2</sub>·xH<sub>2</sub>O obtained fast Zn<sup>2+</sup> diffusion kinetics and outstanding cycling performance, such as 88 mA h g<sup>-1</sup> at 50 A g<sup>-1</sup>. And, Zhang et al. achieved ultrahigh rate capability under the application of pseudocapacitive proton insertion reaction.<sup>[23]</sup>

Usually, the diffusion-controlled Faradaic process and pseudocapacitor-controlled Zn<sup>2+</sup> ion storage process are coexisting in the AVZB and their contribution can be divided as the following equation according to the multiple-scan rate of cyclic voltammetry curve.

$$i = a\nu^b \quad (13)$$

$$i = k_1\nu + k_2\nu^{1/2} \quad (14)$$

where  $a$  and  $b$  are adjustment factor. When  $b$  is 0.5, it shows the diffusion-controlled reaction process, and when  $b$  is 1, it

indicates the pseudocapacitor-controlled Zn<sup>2+</sup> ion storage process. Usually, the value of  $b$  ranges from 0.5 to 1, showing the jointly controlled Zn<sup>2+</sup> ion storage process and its relative contribution can be calculated according to Equation (14). However, researchers only judge the existence of this process and the relative contribution of simple calculations, and there is a lack of necessary and in-depth research on its specific types and detailed energy storage mechanisms in AVZB system.

### 3. Challenges of Zn//VO<sub>2</sub> Battery

Although AVZB has been studied and certain research progress has been made, the challenges encountered by VO<sub>2</sub> in the zinc storage process also need to be analyzed and discussed in depth. The common issues can be concluded, as shown in Figure 5.

#### 3.1. Sluggish Zn<sup>2+</sup>/e<sup>-</sup> Transport Kinetics

VO<sub>2</sub> as an inorganic compound has intrinsic poor conductivity, which is not conducive to the electron transport process (Figure 5a). Moreover, zinc ions usually exist in the form of hydrated [Zn(H<sub>2</sub>O)<sub>6</sub>]<sup>2+</sup> ions with a higher radius (0.55 nm) than Zn<sup>2+</sup> ion (0.076 nm) in aqueous electrolyte, which will greatly

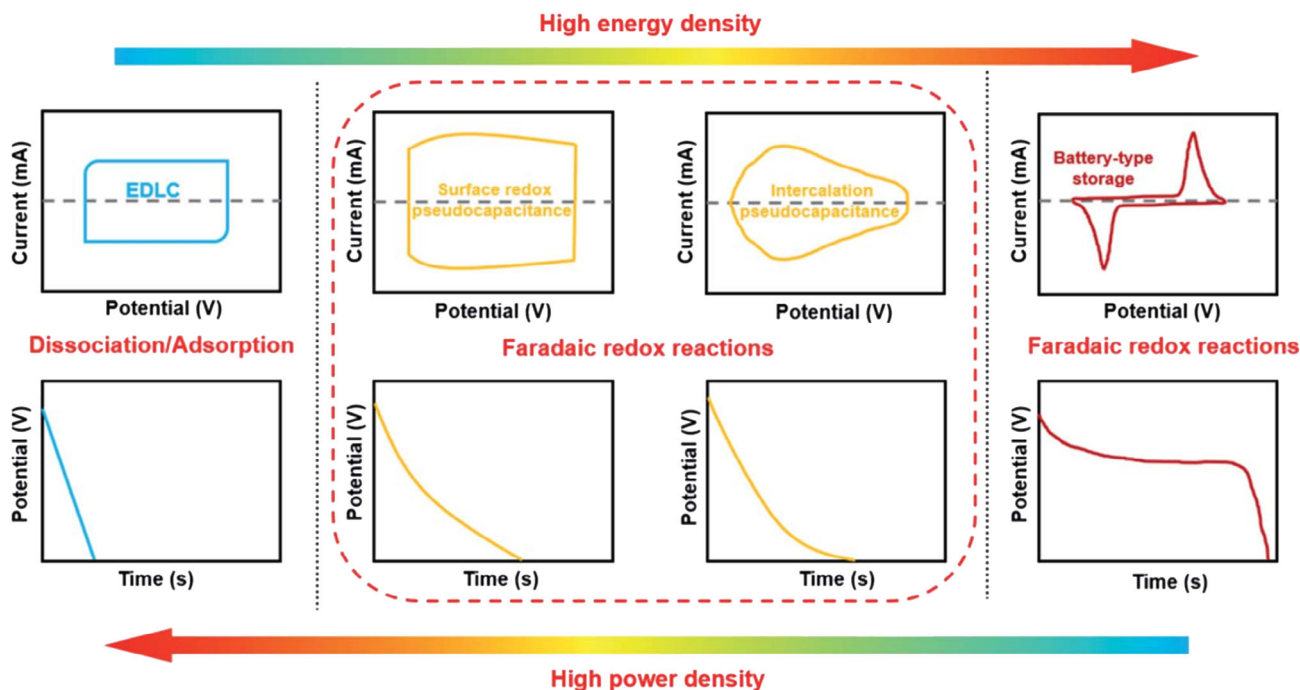


**Figure 4.** CV and  $E-t$  plots of electric double layer capacitors (EDLCs), surface redox pseudocapacitance, intercalation pseudocapacitance, and battery-type storage, respectively. Reproduced with permission.<sup>[13]</sup> Copyright 2022, The Royal Society of Chemistry.

increase the migration resistance during ion transport within electrolyte and desolvation process is required at the electrode/electrolyte interface. And, the  $Zn^{2+}$  ion with a higher charge density than the monovalent ion (e.g.,  $Li^+$ ) shows the sluggish movement within the  $VO_2$  caused by the large electrostatic force between it and the host material. Additionally, the electrode for AVZB is prepared by mixing the  $VO_2$  as active material, binder (such as polyvinylidene fluoride (PVDF) and polytetrafluoroethylene (PTFE)), and conductive agent, where the latter two are inactive and fluorine atoms with high electronegativity also have a greater attraction to zinc ions for occupying and blocking the  $Zn^{2+}$  ion transport path. Usually, this type of issue can be mitigated by adjusting the electrode composition (such as the free-standing electrode) and optimizing the electrolyte as well as other strategies to increase electrical conductivity (such as doped- $VO_2$ ,  $VO_2$ @conductive material composite, etc.).

### 3.2. Structural Collapse and Failure

It can be concluded that the vanadium element will shift to lower binding energy of V–O bond when the  $Zn^{2+}$  ion is inserted into  $VO_2$  from the discussion of  $Zn^{2+}$  ion storage mechanism of  $VO_2$  in the last section, which could cause the structure instability of  $VO_2$  in thermodynamic terms due to the competition between the Zn–O and V–O chemical bond (Figure 5b).<sup>[3d]</sup> The lattice of  $VO_2$  will produce a repeated breathing effect in the subsequent zinc ion insertion/extraction process resulting in stress changes and eventually structural failure (Figure 5b). According to the failure mechanism, it may be solved effectively by the target of weaker interaction between oxygen and  $Zn^{2+}$  ion (typically, oxygen defect or formed charge shield under the help of  $H_2O$

molecule). Also, creating a stronger structure and optimized layer spacing by the conduction of preinserted dopant could break the above dilemma. Moreover, the structural stability can also be maintained via the design of a specific morphology structure or amorphous crystal structure to release stress generated during the repeated insertion/extraction of  $Zn^{2+}$  ion.

### 3.3. Dissolution of Vanadium Element

The vanadium element of host materials including  $VO_2$  could be dissolved at the electrolyte–electrode interface in aqueous electrolyte due to the strong polarity of  $H_2O$  (Figure 5c). Also, the slow dissolution and corrosion could be caused by the reaction of  $H^+$  and  $VO_2$  cathode due to the weakly acidic  $Zn^{2+}$  ion electrolyte, such as typical  $ZnSO_4$ ,  $Zn(CF_3SO_3)_2$ , and others, which will seriously reduce the attenuation capacity and cycle stability, and ultimately affect the commercial application of AVZB in future. Thus, this dissolution of vanadium element first can be slower by optimizing the electrolyte (e.g., eutectic electrolyte) to decrease the proportion or reactivity of free  $H_2O$ . Moreover, strategies such as composite materials including constructing cathode interface phase to avoid direct contact between  $VO_2$  cathode and the electrolyte can also be considered.

### 3.4. Low Voltage Platform and Narrow Electrochemical Working Window

Usually, the energy density mainly is decided by the specific capacity and working voltage of the battery. First, the stable and narrow windows are only 1.23 V mainly caused by due to

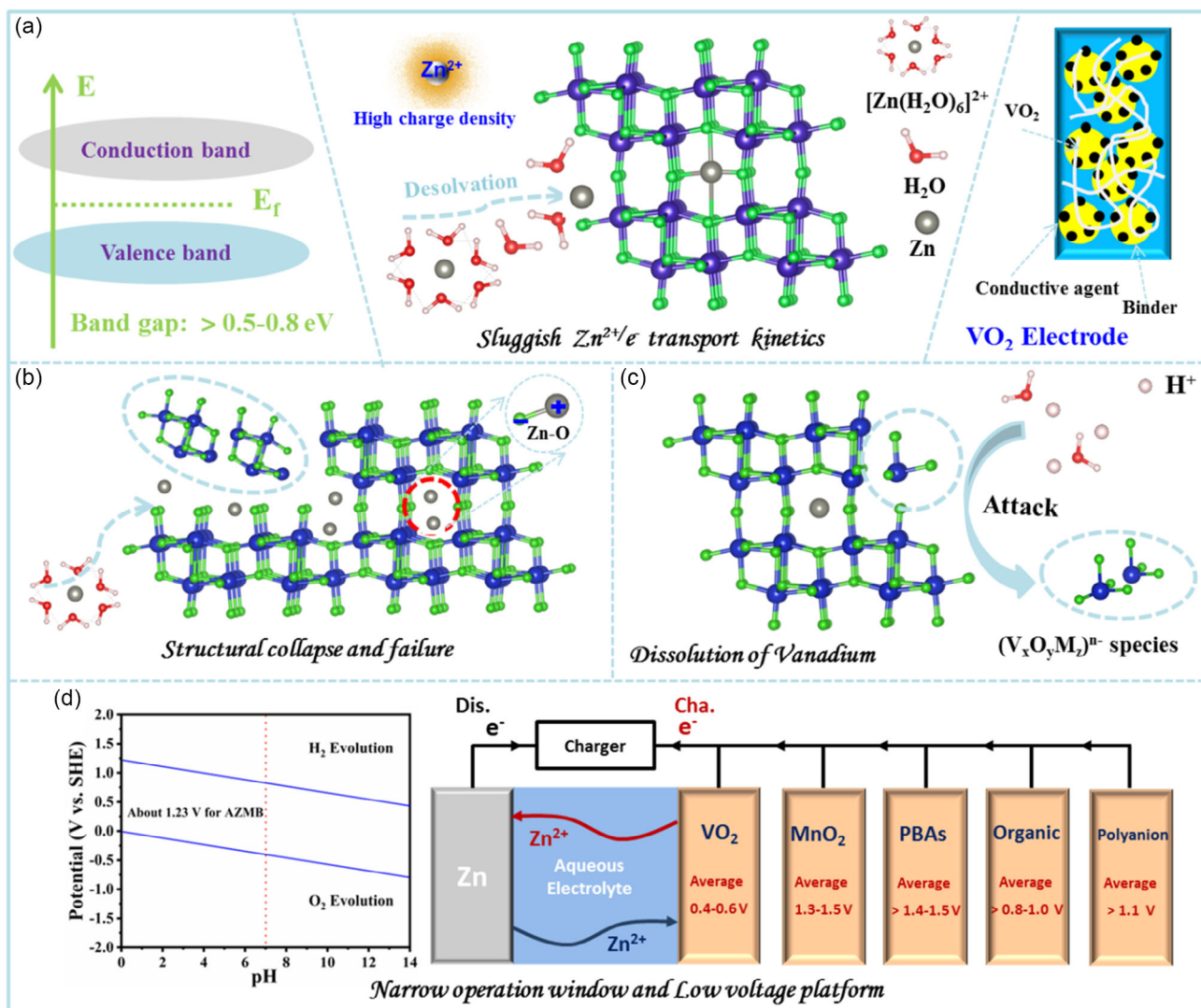


**Figure 5.** The schematic diagram of the main challenges faced by the aqueous Zn- $\text{VO}_2$  battery. a) Sluggish  $\text{Zn}^{2+}/e^-$  transport kinetics. b) Structural collapse and failure. c) Dissolution of vanadium element. d) Low voltage platform and narrow electrochemical working window.

the presence of oxygen evolution reaction (OER) and hydrogen evolution reaction (HER) in water-based electrolytes causing the operating voltage window is always between 0 and 2 V in AVZB. Moreover, the discharge voltage platform is always around 0.4–0.6 V in AVZB system, although the specific capacity of  $\text{VO}_2$  is similar to that of organic electrolyte, which will lead to the inconsiderable energy density (Figure 5d). Thus, how to design a wide window and electrochemically stable electrolyte will most likely alleviate the above problems based on the above discussion of electrolytes. Typically, adjusting the appropriate pH and selecting the appropriate electrolyte salt and electrolyte concentration, etc.

## 4. Advanced Design Strategy

Recently, researchers have made increasing efforts to enhance the ability of  $\text{VO}_2$  to storage  $\text{Zn}^{2+}$  ion in AVZB from the physical/chemical properties (such as crystal structure and

microstructure, etc.) preparation of electrolyte and composition of electrode based on the abovementioned issues of  $\text{VO}_2$ .

### 4.1. Design of Microstructure for $\text{VO}_2$

The morphology structure of the synthesized  $\text{VO}_2$  can be divided into one-dimensional (1D), two-dimensional (2D), and three-dimensional (3D) nanomaterials according to the size in different directions.

Usually, 1D nanomaterials with the nanometer scale dimensions in one direction with long and small structural features including nanowire, nanorod, and nanotube. And, it can guarantee excellent electronic and thermal transport properties as well as excellent mechanical properties (Figure 6a). Ding et al. prepared  $\text{VO}_2(\text{B})$  nanofibers as cathodes for AVZB and delivered outstanding performance (Figure 6b).<sup>[24]</sup> This could be attributed to the nanofibers' structure which can reduce the ion transport

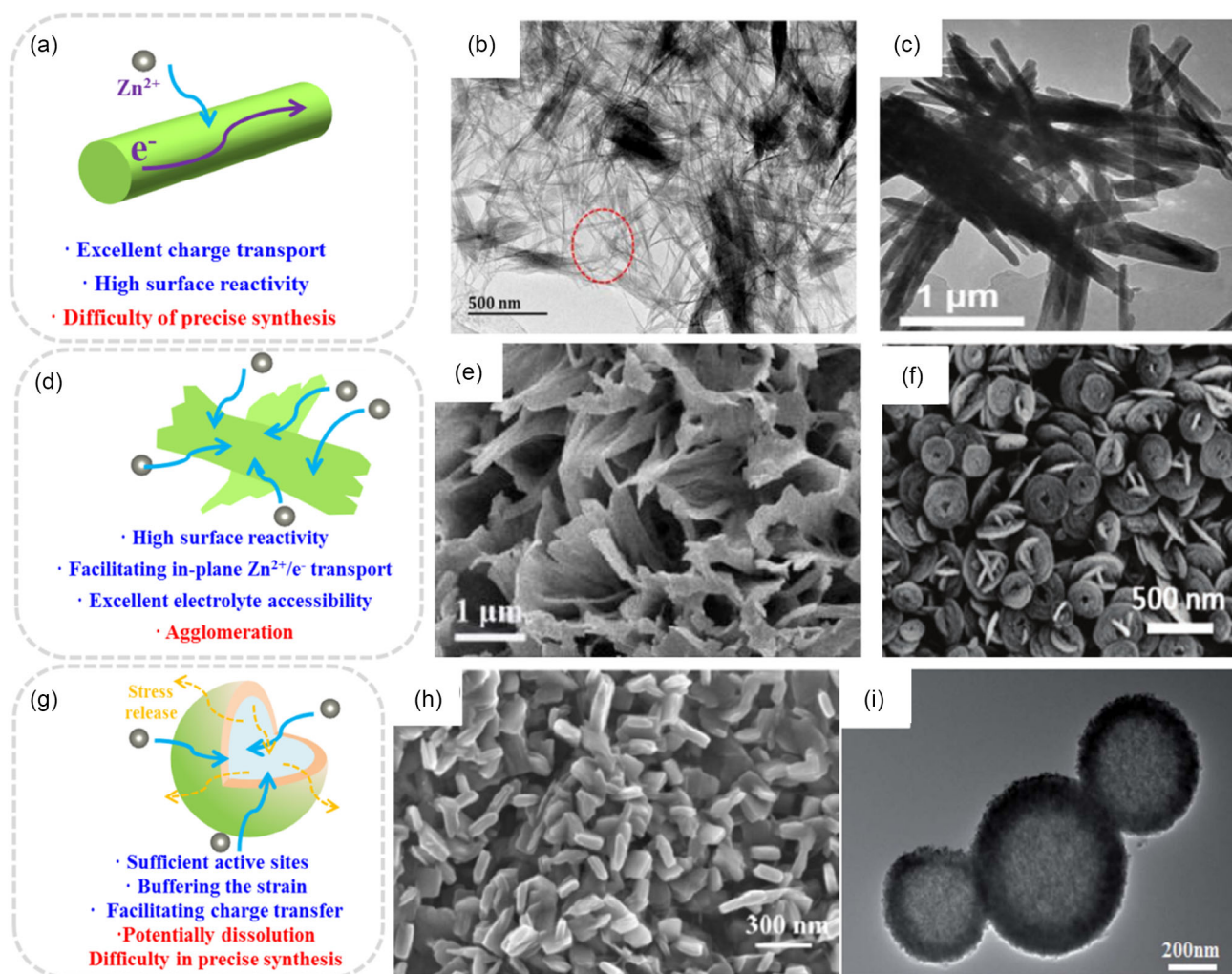


**Figure 6.** The common microstructure of  $VO_2$ . a) The main advantage and disadvantage of  $VO_2$  with nanowires. b) Nanofibers. Reproduced with permission.<sup>[24]</sup> Copyright 2018, Wiley-VCH. c) Nanorods. Reproduced with permission.<sup>[7a]</sup> Copyright 2019, The American Chemical Society. d) The main advantage and disadvantage of  $VO_2$  with nanosheets. e) Nanosheet. Reproduced with permission.<sup>[25]</sup> Copyright 2022, Elsevier. f) Nanoplates. Reproduced with permission.<sup>[7b]</sup> Copyright 2020, Wiley-VCH. g) The main advantage and disadvantage of  $VO_2$  with 3D structure. h) Nanocuboids. Reproduced with permission.<sup>[16c]</sup> Copyright 2019, Springer Nature. i) Hollow nanospheres. Reproduced with permission.<sup>[10a]</sup> Copyright 2019, The Royal Society of Chemistry.

path and provide a more reactive site. In our group, Chen et al.<sup>[7a]</sup> also proposed nanorods  $VO_2(B)$  which can exhibit  $325.6 \text{ mA h g}^{-1}$  at  $50 \text{ mA g}^{-1}$  and excellent average  $Zn^{2+}$  ion diffusion coefficient of  $10^{-6.5} \text{ cm}^2 \text{ s}^{-1}$  (Figure 6c). However, the high specific surface area and unstable mechanical properties could often cause the agglomerate, which may reduce the active site to store  $Zn^{2+}$  ion. And, there are still some difficulties in accurate synthesis, especially at the industrial level.

Moreover, the 2D nanosheet with the size within the nanometer scale along the Z axis. In general, its large specific surface area can increase the contact area between the electrode and the electrolyte, which will greatly increase the adsorption site of zinc ions, reduce the diffusion distance, and allow the in-plane  $Zn^{2+}/e^-$  transport (Figure 6d). Bai et al. synthesized  $VO_2(B)$  nanoflakes with petal-shaped folds and provided high-specific capacity and excellent rate performance (Table 1), which can

be attributed to the much increased conducted area for shorten the migration path between the  $VO_2$  electrode and electrolyte (Figure 6e).<sup>[25]</sup> Cao et al.<sup>[7b]</sup> developed  $VO_2(D)$  with ancient Chinese coin-shape via the localized Ostwald ripening-guided dissolution/regrowth (Figure 6f), which had obtained high-specific capacity of  $394 \text{ mA h g}^{-1}$  at  $0.1 \text{ A g}^{-1}$ , outstanding long-term cycling performance and faster kinetics via the enhanced mass transfer process due to the induced abundant electrolyte-accessible sites and transfer pathways. However, the thinner sheet structures will have an obvious tendency to adsorb each other and stick due to the larger surface energy and the presence of van der Waals forces, which may reduce the adsorption site of zinc ions and prevent ion diffusion.

Additionally,  $VO_2$  with 3D structure including mainly 3D networks and hollow nanospheres also has been developed and delivered outstanding performance in AVZB. Compared with



**Table 1.** The energy storage mechanism and typical performance of VO<sub>2</sub> with different modification strategies.

Material and microstructure	Charge ion	Specific capacity of a mA h g <sup>-1</sup> at b A g <sup>-1</sup>	Cycling performance	Others performance	References
VO <sub>2</sub> (A)-hollow nanospheres	Zn <sup>2+</sup>	357 at 0.1	76%, 500 cycles at 5 A g <sup>-1</sup>	6.8 × 10 <sup>-10</sup> -1.1 × 10 <sup>-10</sup> cm <sup>2</sup> s <sup>-1</sup>	[10a]
VO <sub>2</sub> (D) nanoplates with ancient Chinese coins shape	Zn <sup>2+</sup>	397.4 at 0.1; 183.9 at 3	81.2%, 1200 cycles at 3 A g <sup>-1</sup>	275.8 Wh kg <sup>-1</sup> at 70 W kg <sup>-1</sup>	[7b]
VO <sub>2</sub> (D) hollow nanospheres	To V <sub>2</sub> O <sub>5</sub> ·xH <sub>2</sub> O; Zn <sup>2+</sup> /H <sup>+</sup>	408 at 0.1; 200 at 20	Capacity fading rate of 0.0023% per cycle at 10 A g <sup>-1</sup> , 30 000 cycles	125.1 W h kg <sup>-1</sup> at 12512.3 W kg <sup>-1</sup>	[11]
N-VO <sub>2</sub> (M)@NC@CNTF	Zn <sup>2+</sup> /H <sup>+</sup>	441.383 mA h cm <sup>-3</sup> at	96.70%, 4000 bending cycles	313.13 mWh cm <sup>-3</sup>	[10b]
VO <sub>2</sub> (M)@PPY hollow nanospheres	Zn <sup>2+</sup>	440, 0.1	143 mA h g <sup>-1</sup> after 860 cycles at 1 A g <sup>-1</sup>	316.8 Wh kg <sup>-1</sup> at 71.7 W kg <sup>-1</sup>	[26]
VO <sub>2</sub> (M)/CNT film	H <sup>+</sup> /Zn <sup>2+</sup>	248 at 2; 194.9 at 40	84.5%, 5000 cycles at 20 A g <sup>-1</sup>	10 <sup>-9</sup> -10 <sup>-8</sup> cm <sup>2</sup> s <sup>-1</sup>	[23]
Cubic-layered VO <sub>2</sub>	To Zn <sub>2</sub> V <sub>2</sub> O <sub>7</sub> ; H <sup>+</sup> /Zn <sup>2+</sup>	329.8 at 0.1	241.7 mA h g <sup>-1</sup> after 4000 cycles at 10 A g <sup>-1</sup>	7 × 10 <sup>-11</sup> -3.2 × 10 <sup>-12</sup> cm <sup>2</sup> s <sup>-1</sup>	[19b]
VO <sub>2</sub> (B) nanofibers	Zn <sup>2+</sup>	357, 0.25C	171 at 300C	10 <sup>-12</sup> -10 <sup>-11</sup> cm <sup>2</sup> s <sup>-1</sup>	[24]
VO <sub>2</sub> (B) nanorods	Zn <sup>2+</sup>	325.6 at 0.05	86%, 5000 cycles at 3.0 A g <sup>-1</sup>	10 <sup>-5.6</sup> -10 <sup>-7.5</sup> cm <sup>2</sup> s <sup>-1</sup>	[7a]
VO <sub>2</sub> (B) nanorods	To Zn <sub>3</sub> (OH) <sub>2</sub> V <sub>2</sub> O <sub>7</sub> ·2H <sub>2</sub> O; H <sup>+</sup> /Zn <sup>2+</sup>	330 at 0.1; 130 at 10	-	10 <sup>-11</sup> -10 <sup>-12</sup> cm <sup>2</sup> s <sup>-1</sup>	[19c]
VO <sub>2</sub> (B) nanorods	H <sup>+</sup>	About 250 at 1	75.5%, 945 cycles at 3.0 A g <sup>-1</sup>	-	[15]
VO <sub>2</sub> (B)-0.2H <sub>2</sub> O nanocuboids/rGO	Zn <sup>2+</sup> /H <sub>2</sub> O	423 at 0.25	87%, 1000 cycles at 8.0 A g <sup>-1</sup>	-	[16c]
VO <sub>2</sub> (B) nanoflakes	-	301.7 at 1; 89 at 50	201.3 mA h g <sup>-1</sup> after 2000 cycles at 10 A g <sup>-1</sup>	-	[25]
Argon-treated VO <sub>2</sub> (B) microsphere	To V <sub>2</sub> O <sub>5</sub> ·xH <sub>2</sub> O; Zn <sup>2+</sup>	446 at 0.1; 323 at 10	194 mA h g <sup>-1</sup> after 4000 cycles at 20 A g <sup>-1</sup>	10 <sup>-10</sup> cm <sup>2</sup> s <sup>-1</sup>	[17]
Holey C@VO <sub>2</sub> (B)	H <sup>+</sup> /Zn <sup>2+</sup>	386.9 at 0.2; 332 at 5	84.3%, 600 cycles at 5.0 A g <sup>-1</sup>	-	[32]
VO <sub>2</sub> (B)@ZnO	-	365 at 0.5	54 %, 500 cycles at 5.0 A g <sup>-1</sup>	Against vanadium dissolution	[35]
VO <sub>2</sub> (B)@C	Zn <sup>2+</sup>	400 at 0.2	260 mA h g <sup>-1</sup> after 1000 cycles at 5.0 A g <sup>-1</sup>	280 W h kg <sup>-1</sup> at 140 W kg <sup>-1</sup> ; soft pack batteries	[69]
VO <sub>2</sub> (B)@N-doped carbon	Zn <sup>2+</sup>	435.4 at 1	268.5 mAh g <sup>-1</sup> after 2500 cycles at 10.0 A g <sup>-1</sup>	238.0 Wh kg <sup>-1</sup> at 7.0 kW kg <sup>-1</sup>	[34]
C@VO <sub>2</sub> (B)	H <sup>+</sup> /Zn <sup>2+</sup>	281 at 0.2	95.4%, 1000 cycles at 5.0 A g <sup>-1</sup>	4 × 10 <sup>-11</sup> -6 × 10 <sup>-13</sup> cm <sup>2</sup> s <sup>-1</sup>	[33]
Freestanding VO <sub>2</sub> (B)/MXene	-	228.5 at 0.2	over 126.6 mA h g <sup>-1</sup> after 700 cycles at 2 A g <sup>-1</sup>	72.1%, 2500 cycles at 5.0 A g <sup>-1</sup> quasi-solid-state ZIBs	[68]
Flower-like MXene@VO <sub>2</sub> (B) clusters	Zn <sup>2+</sup>	363.2 at 0.2C; 169.1 at 50C	76%, 5000 cycles at 20C	Suppressed vanadium dissolved	[31]
VO <sub>2</sub> (B)@rGO	Zn <sup>2+</sup>	170 at 0.5 C	131 mAh g <sup>-1</sup> after 200 cycles at	10 <sup>-8</sup> -10 <sup>-11</sup> S cm <sup>-1</sup>	[70]
Freestanding graphene/VO <sub>2</sub> (B)	Zn <sup>2+</sup>	About 260 at 0.1	99%, 1000 cycles at 4 A g <sup>-1</sup>	Soft-packaged Zn/VO <sub>2</sub> battery	[7c]
VO <sub>2</sub> (B)-Ti	H <sup>+</sup> /Zn <sup>2+</sup>	325 at 0.1	239 mAh g <sup>-1</sup> after 550 cycles at 1 A g <sup>-1</sup>	-	[14]
VO <sub>2</sub> (B) nanobelts @rGO	Zn <sup>2+</sup>	456 at 0.1	283 mAh g <sup>-1</sup> after 1000 cycles at 5 A g <sup>-1</sup>	10 <sup>-12.5</sup> -10 <sup>-11.5</sup> cm <sup>2</sup> s <sup>-1</sup>	[28]
VO <sub>2</sub> (B)-0.26H <sub>2</sub> O nanobelts @rGO	Zn <sup>2+</sup>	373 at 0.1	225 mA h g <sup>-1</sup> after 1200 cycles at 5 A g <sup>-1</sup>	10 <sup>-9</sup> -10 <sup>-10</sup> cm <sup>2</sup> s <sup>-1</sup>	[27]
Oxygen-deficient VO <sub>2</sub> (B)/G nanobelts	To V <sub>2</sub> O <sub>5</sub> ·xH <sub>2</sub> O; Zn <sup>2+</sup>	731 at 0.1	350 mAh g <sup>-1</sup> after 1000 cycles at 5 A g <sup>-1</sup>	Average 10 <sup>-9</sup> cm <sup>2</sup> s <sup>-1</sup>	[18]
VO <sub>2</sub> (B)@CFS	-	386.2 at 0.2	153.9 mA h g <sup>-1</sup> after 1000 cycles at 2 A g <sup>-1</sup>	10 <sup>-9</sup> -10 <sup>-8</sup> cm <sup>2</sup> s <sup>-1</sup>	[30]
V <sub>O</sub> ••-VO <sub>2</sub> (B)	-	375 at 0.1	175 mA h g <sup>-1</sup> at 5 A g <sup>-1</sup> over 2000 cycles	-	[40]
VO <sub>1.88</sub> (B) nanobelts	Zn <sup>2+</sup>	360 at 0.1	About 150 mA h g <sup>-1</sup> after 700 cycles at 3 A g <sup>-1</sup>	250 mA h g <sup>-1</sup> at 0.1 A g <sup>-1</sup> with 4 mg cm <sup>-2</sup>	[10c]
O <sub>d</sub> -VO <sub>2</sub> (B)-rGO	Zn <sup>2+</sup>	376 at 0.1 116 at 20	88.6%, 5000 cycles at 10 A g <sup>-1</sup>	10 <sup>-9</sup> -10 <sup>-8</sup> cm <sup>2</sup> s <sup>-1</sup>	[42]
O <sub>d</sub> -VO <sub>2</sub> (B)-xH <sub>2</sub> O/rGO	H <sup>+</sup> /Zn <sup>2+</sup>	428.6 at 0.1; 186 at 20	197.5 mA h g <sup>-1</sup> at 10 A g <sup>-1</sup> after 2000 cycles	245.3 Wh kg <sup>-1</sup> at 245.3 Wh kg <sup>-1</sup> ; flexible soft pack battery	[43]
O <sub>d</sub> -VO <sub>2</sub> (B)	Zn <sup>2+</sup>	380 at 0.2	92.6%, 2000 cycles at 3 A g <sup>-1</sup>	197 Wh kg <sup>-1</sup> at 0.641 W kg <sup>-1</sup> ;	[41]

**Table 1.** Continued.

Material and microstructure	Charge ion	Specific capacity of a mA h g <sup>-1</sup> at b A g <sup>-1</sup>	Cycling performance	Others performance	References
VO <sub>x</sub> -G heterostructure	Zn <sup>2+</sup>	443 at 0.1; 174.4 at 100	Average 300 after 1000 cycles at 10 A g <sup>-1</sup>	Capacity retention of 39.4% for a 1000-fold increase in current density	[55b]
Heterostructured VO <sub>2</sub> (B) @CC	Zn <sup>2+</sup>	350 at 0.1	150 mA h g <sup>-1</sup> after 4500 cycles at 4 A g <sup>-1</sup>	Average 10 <sup>-7</sup> cm <sup>2</sup> s <sup>-1</sup>	[55a]
VO <sub>2</sub> (B)@V <sub>2</sub> C 1D/2D heterostructure	-	456 at 0.5	81%, 1000 cycles at 5 A g <sup>-1</sup>	About 10 <sup>-9.5</sup> cm <sup>2</sup> s <sup>-1</sup>	[56a]
C@VO <sub>2</sub> @V <sub>2</sub> O <sub>5</sub>	H <sup>+</sup> /Zn <sup>2+</sup>	376 at 0.05; 178 at 5	90.3%, 2000 cycles at 5 A g <sup>-1</sup>	5.4 × 10 <sup>-8</sup> cm <sup>2</sup> s <sup>-1</sup>	[58]
3D bird nest-like VO <sub>2</sub> /MXene	Zn <sup>2+</sup>	445 at 0.4	82%, over 2500 cycles at 20 A g <sup>-1</sup>	247.2 mA h g <sup>-1</sup> at 5.0 A g <sup>-1</sup> at -20 °C	[56c]
VO <sub>2</sub> (B)@Ta <sub>4</sub> C <sub>3</sub>	Zn <sup>2+</sup>	437 at 0.1	78.2%, 2000 cycles at 1 A g <sup>-1</sup>	-	[56b]
V <sub>0</sub> -VO <sub>2</sub> (B)/MXene	H <sup>+</sup> /Zn <sup>2+</sup>	320 at 0.1	253 mA h g <sup>-1</sup> after 3000 cycles at 10 A g <sup>-1</sup>	10 <sup>-10</sup> -10 <sup>-11</sup> cm <sup>2</sup> s <sup>-1</sup>	[71]
Ni-VO <sub>2</sub> (B)	H <sup>+</sup> /Zn <sup>2+</sup>	312 at 0.05; 182 at 5	130.6 mA h g <sup>-1</sup> at 10 A g <sup>-1</sup> after 2000 cycles	127 mA h g <sup>-1</sup> at 1 A g <sup>-1</sup> after 1000 cycles in soft-packaged battery	[44]
Porous W-VO <sub>2</sub> (B) nanosheet	H <sup>+</sup> /Zn <sup>2+</sup>	346 at 0.1; 221 at 10	76.4%, 1000 cycles at 4 A g <sup>-1</sup>	10 <sup>-9</sup> -10 <sup>-8</sup> cm <sup>2</sup> s <sup>-1</sup>	[45]
W-VO <sub>2</sub> (B)	Zn <sup>2+</sup>	235 at 0.5	118 mA h g <sup>-1</sup> at 10 A g <sup>-1</sup> after 2000 cycles	2.85 × 10 <sup>-4</sup> s cm <sup>-1</sup>	[46]
Mo-VO <sub>2</sub> (B)	Zn <sup>2+</sup>	Average 320 at 0.1	81.4%, 3000 cycles at 3 A g <sup>-1</sup>	2.1 × 10 <sup>-8</sup> cm <sup>2</sup> s <sup>-1</sup>	[47]
H-VO <sub>2</sub> (B)	Zn <sup>2+</sup>	572 at 0.2	About 80 mA h g <sup>-1</sup> after 22 000 cycles at 10 A g <sup>-1</sup>	443 Wh kg <sup>-1</sup> at 0.2 A g <sup>-1</sup>	[52a]
K-VO <sub>2</sub> (B)	Zn <sup>2+</sup>	350 at 0.5; 122 at 50	80%, 3000 cycles at 20 A g <sup>-1</sup>	3.9 × 10 <sup>-12</sup> cm <sup>2</sup> s <sup>-1</sup>	[52b]
H <sup>+</sup> /Na <sup>+</sup> -VO <sub>2</sub> (B)	H <sup>+</sup> /Zn <sup>2+</sup>	345 at 0.2	118 mA h g <sup>-1</sup> after 3000 cycles at 12 A g <sup>-1</sup>	10 <sup>-10</sup> -10 <sup>-9</sup> cm <sup>2</sup> s <sup>-1</sup>	[51]
PVP-modified Mn-VO <sub>2</sub> (B)	Zn <sup>2+</sup>	419.89 at 0.5; 328.06 at 10	176.5 mA h g <sup>-1</sup> after 5000 cycles at 10 A g <sup>-1</sup>	1.74 × 10 <sup>-10</sup> -1.22 × 10 <sup>-9</sup> cm <sup>2</sup> s <sup>-1</sup>	[53]
Mn-VO <sub>2</sub> (B)	To Zn <sub>0.25</sub> V <sub>2</sub> O <sub>5</sub> ·nH <sub>2</sub> O H <sup>+</sup> /Zn <sup>2+</sup>	413.4 at 0.1	80.7%, 10 000 cycles at 5 A g <sup>-1</sup>	5.17 × 10 <sup>-11</sup> -1.62 × 10 <sup>-10</sup> cm <sup>2</sup> s <sup>-1</sup>	[19a]
Mn-VO <sub>2</sub> (B)	Zn <sup>2+</sup> and [Zn(H <sub>2</sub> O) <sub>6</sub> ] <sup>2+</sup>	462.5 at 0.1	120 mA h g <sup>-1</sup> after 2500 cycles at 5 A g <sup>-1</sup>	10 <sup>-9</sup> -10 <sup>-12</sup> cm <sup>2</sup> s <sup>-1</sup>	[16a]
B-VO <sub>2</sub> (B)	Zn <sup>2+</sup>	281.7 at 0.1; 142.2 at 20	133.3 mA h g <sup>-1</sup> after 1000 cycles at 5 A g <sup>-1</sup>	10 <sup>-12</sup> -10 <sup>-11</sup> cm <sup>2</sup> s <sup>-1</sup>	[48]
N-VO <sub>2</sub> (B) nanobelts	H <sup>+</sup> /Zn <sup>2+</sup>	352.3 at 0.1	189.6 and 123.9 mA h g <sup>-1</sup> over 2000 cycles at 2 and 5 A g <sup>-1</sup>	4.2 × 10 <sup>-10</sup> cm <sup>2</sup> s <sup>-1</sup>	[49]
PANI-VO <sub>2</sub> (B)	Zn <sup>2+</sup>	415 at 0.1	173 mA h g <sup>-1</sup> after 1000 cycles at 2 A g <sup>-1</sup>	6.15 × 10 <sup>-9</sup> -1.55 × 10 <sup>-10</sup> cm <sup>2</sup> s <sup>-1</sup>	[72]
Zn(ClO <sub>4</sub> ) <sub>2</sub>	-	240 at 0.5	About 150 mA h g <sup>-1</sup> after 500 cycles at 2 A g <sup>-1</sup>	3000 h at 1 mA cm <sup>-2</sup> with 1 mA h cm <sup>-2</sup>	[63]
Zn(CF <sub>3</sub> SO <sub>3</sub> ) <sub>2</sub> -PVA hydrogel electrolyte	-	314.7 μA h cm <sup>-2</sup> at 0.14 mA cm <sup>-2</sup>	71.8%, 200 cycles at 3.14 mA cm <sup>-2</sup>	Good flexibility at 150° and high-temperature stability at 100 °C	[64]
ZnSO <sub>4</sub> + ZnI <sub>2</sub>	H <sup>+</sup> /Zn <sup>2+</sup> /I <sup>-</sup>	260 at 0.3	322.4 after 2000 cycles at 2 A g <sup>-1</sup>	Open-circuit voltage (OCV) from 1.15 to 1.3 V	[73]
2M Zn(OTf) <sub>2</sub> + 8M LiOTf	-	Average 260 at 0.1 98.2% over 400	89.7% over 10 000 cycles at 10 A g <sup>-1</sup>	98.7% after 500 cycles at 1 A g <sup>-1</sup> in pouch cell	[66]
EDTA-3Na-ZnSO <sub>4</sub>	-	403.6 at 1; 297.6 at 8	281.5 after 1000 cycles at 5 A g <sup>-1</sup>	2.02E <sup>-10</sup> -2.27E <sup>-9</sup>	[67]

the 1D and 2D materials mentioned above, it has a more uniform distribution property in space. The above structural advantages enable the 3D structured material to effectively reduce the agglomeration problem of low-dimensional materials, and its unique spatial structure also helps to facilitate electrolyte

accessibility, as well as alleviate the stress changes generated during the insertion/removal of Zn<sup>2+</sup> ions, thus achieving to maintain structural stability (Figure 6g). VO<sub>2</sub> with hollow nanospheres has been demonstrated that it can own excellent cycling stability and fast ion diffusion kinetics (Table 1, Figure 6h).<sup>[11,25,26]</sup>

This modification mechanism can be understood as reducing the agglomeration of low-dimensional materials, providing enough space to enrich the contact area for facilitating the  $\text{Zn}^{2+}$  ion diffusion, and relieving the stress during the  $\text{Zn}^{2+}$  ion insertion/extraction process. Similarly, the  $\text{VO}_2\cdot 0.2\text{H}_2\text{O}$  nanocuboids composited with rGO also exhibited the same modification results of excellent electronic and ionic transport ability, thus achieved high-specific capacity and capacity retention (Table 1) as well as faster ion/electron transport process (Figure 6).<sup>[16c]</sup> However, 3D structure may face the challenge of potential dissolution and produce other inactive side-production after excessive contact with weakly acidic aqueous electrolyte. Also, there is existing difficulty in precise and uniform synthesis at the factory level.

Basely, it can be found that the increased contact area between  $\text{VO}_2$  and electrolyte can shorten the ion path, induce more  $\text{Zn}^{2+}$  ion adsorb site for increased pseudocapacitor-controlled contribution, and buffer stress change respectively for maintaining structural stability when the  $\text{VO}_2$  has differently special morphology structure. Thus, the significantly enhanced zinc ion storage ability of the  $\text{VO}_2$  cathode material could be achieved well. However, we must also clearly recognize that how to control the synthesis of these  $\text{VO}_2$  with special morphology and structure on a large scale and at a low cost is still a topic worthy of in-depth discussion.

## 4.2. Composite Strategy for $\text{VO}_2$ Cathode

Usually, composite materials are prepared by combining two or more materials with different properties through physical or chemical methods. Various materials can produce a synergistic effect by their special performance, which will lead to the better comprehensive performance of composite materials than the original materials. Moreover, the awkward electrical conductivity of  $\text{VO}_2$  can lead to large polarization and poor rate performance. The elaborate microstructure and lattice of  $\text{VO}_2$  will be destroyed for the attenuation of performance in the process of repetitive  $\text{Zn}^{2+}$  ion insertion/extraction. Also, the vanadium-dissolution of the  $\text{VO}_2$  cathode material during the cycle will also lead to problems such as rapid capacity decay.

### 4.2.1. Composite Strategies with Conductive Materials

Pertinently, research has found that combining  $\text{VO}_2$  with a conductive compound could effectively alleviate these problems at the same time according to the advantages of composite materials. In this case, carbon-based materials become the most popular and common reinforcement component materials due to the typical characteristic of excellent electronic conductivity. Xie et al. prepared  $\text{VO}_2\cdot 0.26\text{H}_2\text{O}$  nanobelts@reduced graphene oxides to store  $\text{Zn}^{2+}$  ions in AVZB (Figure 7a).<sup>[27]</sup> Compared to the pure  $\text{VO}_2$ , the  $\text{VO}_2\cdot 0.26\text{H}_2\text{O}@r\text{GO}$  delivers high-specific capacity, superior capacity retention rate of 94.9% after over 2000 cycles at  $0.1\text{ A g}^{-1}$ , and faster  $\text{Zn}^{2+}$  transfer kinetics (Table 1). It can not only be attributed to the large surface area of  $\text{VO}_2$  nanobelts for the increased reactive sites, but also provided enhanced electronic transport pathway by the reduction of graphene oxides. Moreover, the surface functional groups of graphene oxides

could participate in the reaction process for the much extra pseudocapacitor-controlled capacity and the soft graphene oxides also can act as a buffer to accommodate the considerable stress generated during the insertion/extraction of zinc ions into/from  $\text{VO}_2$  cathode for more stable structure.<sup>[28]</sup> Cui et al.<sup>[28]</sup> recently also proposed  $\text{VO}_2(\text{B})$  nanobelts@rGO composites as cathode for AVZB, which not only obtained remarkable rate performance and durable long cycle ability (Table 1), but also achieved considerable surface-controlling contribution of 89% even at  $0.1\text{ mV s}^{-1}$ .

Notably, the freestanding  $\text{VO}_2$ @conductive materials also can be obtained and retain the advantages of conductive materials for AVZB under the action of different preparation method, which can avoid the inactive binders and unsatisfactory porous structure within the traditional electrode (Figure 7b,c).<sup>[29]</sup> The free-standing graphene/ $\text{VO}_2$  films had been prepared as promising cathode for AVZB via the combination of freeze-drying, high-temperature reduction, and mechanical compression, which not only shows excellent zinc storage capacity in conventional cell batteries, but also exhibits great application potential in the field of flexible soft-pack batteries.<sup>[7c]</sup> In this case, the rGO with self-assembled 3D macroscopic porous architectures can produce space for filling active materials and also plays the role of current collectors for accelerating  $\text{Zn}^{2+}$  ion/electron transportation. In addition, this type of self-supporting  $\text{VO}_2$  cathode could save the preparation time and reduce the use of the toxic organic dispersants. Moreover, another common carbon-based material of carbon fiber can also be used as the substrate to prepare binder-free  $\text{VO}_2$  electrodes for future deformable and wearable devices due to the carbon fiber has excellent chemical stability, flexibility and excellent electrical conductivity, and other advantages (Figure 7d).<sup>[30]</sup>

Similarly, MXene, as a recently developed 2D transition metal carbides/nitrides compounds since 2011, has been applied in the energy storage field well based on the consideration of advantages, such as excellent metallic conductivity, alterable interlayer spacing and large specific surface area, etc. Thus, the monodispersed flower-like MXene@ $\text{VO}_2$  clusters composite and flexible free-standing  $\text{VO}_2/\text{MXene}$  conductive films with 3D conductive network also had been proposed for AVZB to deliver outstanding  $\text{Zn}^{2+}$  ion storage ability and accelerated ion/ $e^-$  transport process (Figure 7e–g).<sup>[31]</sup>

This composite strategy with conductive materials including the free-standing electrode has the obvious advantage of enhanced ion/ $e^-$  transport for the improvement of cycling performance. However, these conductive materials often are inactive for little ability to store zinc ions, and also reduce the proportion of active materials to the disadvantage of improving the overall energy density in AVZB. Moreover, the contact of  $\text{VO}_2$  and conductive materials is limited and sometimes uneven in the above-mentioned mixing strategy, which will lead to the unsatisfactory modification results (Figure 7a,e–g).

### 4.2.2. Coating Strategy

Currently, the coating strategy has sparked interest among researchers in terms of electrode modification based on the fact that it simultaneously can be beneficial to interface transmission

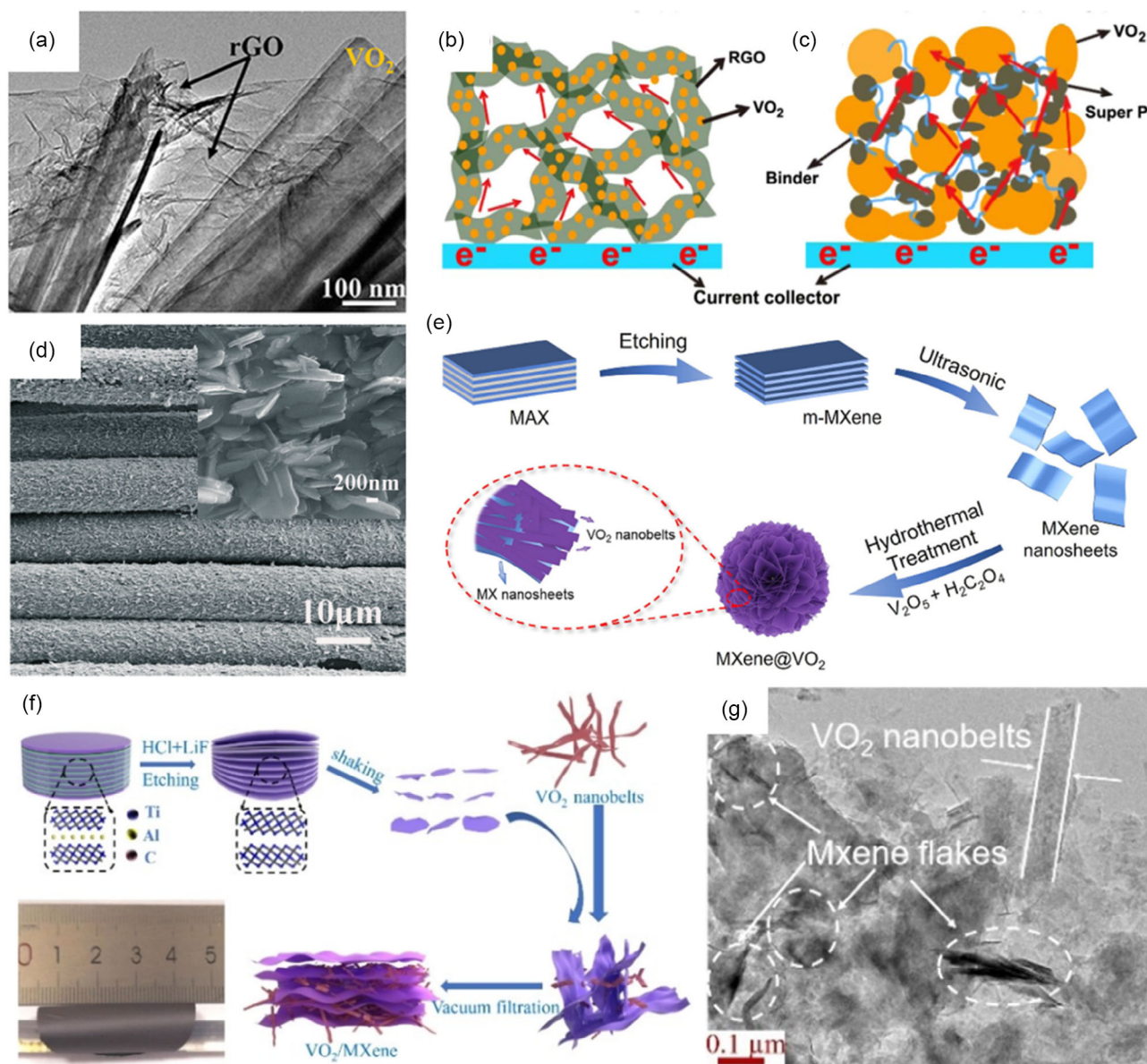


**Figure 7.** a)  $\text{VO}_2$ @rGO composite. Reproduced with permission.<sup>[27]</sup> Copyright 2022, The Royal Society of Chemistry. b,c) Schematic illustration of electron transport in binder-free  $\text{VO}_2$  and traditional  $\text{VO}_2$  electrodes. Reproduced with permission.<sup>[7c]</sup> Copyright 2019, Elsevier. d) Freestanding  $\text{VO}_2$ @Carbon fiber electrode. Reproduced with permission.<sup>[30]</sup> Copyright 2021, The Royal Society of Chemistry. e)  $\text{VO}_2$ @MXene. Reproduced with permission.<sup>[31]</sup> Copyright 2022, The Royal Society of Chemistry. f) Freestanding  $\text{VO}_2$ @MXene electrode and g) corresponding TEM. Reproduced with permission.<sup>[68]</sup> Copyright 2021, Wiley-VCH.

and  $\text{VO}_2$  structure stability. The carbon-based coating, conductive organic layer, and metal oxide layer have been widely used in surface coating modification. Regrettably, these coating layers do not improve ion and electron transport dynamics at the same time, for example, carbon-based materials are good for electron transport and poor ion transport, causing the limited enhancement of  $\text{Zn}^{2+}$  ion storage ability in AVZB. Yang et al.<sup>[32]</sup> recently obtained the holey  $\text{C}@\text{VO}_2$  with unique morphology and interface modification after the alkaline etching treatment, which achieved high capacity retention rate of 84.3% after 600 cycles at  $5 \text{ A g}^{-1}$ . Notably, the lower charge transfer resistance and

faster  $\text{Zn}^{2+}$  ion diffusion in holey  $\text{C}@\text{VO}_2$  also obtained accompanying outstanding cycling performance than pure  $\text{VO}_2$ . This superior  $\text{Zn}^{2+}$  storage ability in the former should be attributed to the holey structure for enriching active site and shortening diffusion path and surface carbon coating for accelerating electron transfer and electrolyte penetration at interface (Figure 8a). Similarly, the  $\text{C}@\text{VO}_2$  cathode with antiaggregation growth and hierarchical porous carbon encapsulation had been prepared as a cathode for AVZB and provided superior storage capability (Table 1), where the reduced aggregation, abundant ion accessible site, and faster transport kinetics can

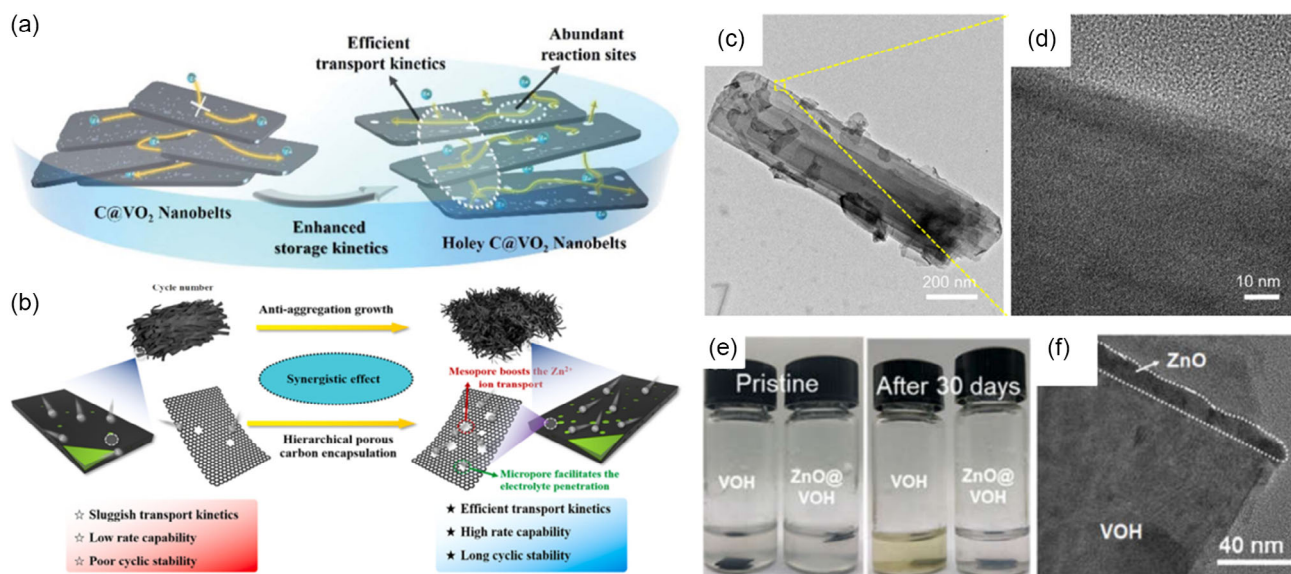


**Figure 8.** a) Schematic diagram of the enhanced storage kinetics mechanism of the holey C@VO<sub>2</sub> electrode. Reproduced with permission.<sup>[32]</sup> Copyright 2021, The Royal Society of Chemistry. b) The comparison of self-aggregation and antiaggregation in two electrodes. Reproduced with permission.<sup>[33]</sup> Copyright 2022, Elsevier. c,d) TEM of VO<sub>2</sub>@ amorphous N-doped carbon. Reproduced with permission.<sup>[34]</sup> Copyright 2022, Elsevier. e) Digital images of suppressing vanadium immersed in the electrolyte and f) TEM of VO<sub>2</sub>@ZnO. Reproduced with permission.<sup>[35]</sup> Copyright 2022, The American Chemical Society.

be responsible for the above outstanding performance (Figure 8b).<sup>[33]</sup>

Moreover, amorphous materials have been designed in field energy storage based on the common advantages of numerous isotropic charge ion diffusion pathways and vacancies as well as relief of stress. Thus, the composite of VO<sub>2</sub> and amorphous N-doped carbon delivers superior Zn<sup>2+</sup> ion storage ability and accelerated Zn<sup>2+</sup>/e<sup>-</sup> transfer kinetics (Figure 8c,d), such as high reversible capacity and capacity retention rate as well as promising energy/power density (Table 1).<sup>[34]</sup> It is worth noting that N-element doping also further improves the conductivity of disordered carbon due to the restructuring of the electronic structure.

Besides, metal oxide can alleviate the problem of slow ion transport in carbon-based materials and is applied in the field of energy storage. Shuai et al. recently prepared ZnO@VO<sub>2</sub>·xH<sub>2</sub>O with uniform and ultrathin ZnO layer by the atomic layer deposition technology with the advantage of easy control of thickness (Figure 8e).<sup>[35]</sup> This artificial interface layer not only allows the Zn<sup>2+</sup> ion to pass through, but also prevents unnecessary side reactions at the electrode interface and inhibits the dissolution of vanadium (Figure 8f). The O and Zn vacancy defects in ZnO also provide an ion diffusion pathway to produce significantly enhanced performance (Table 1).

This coating strategy still needs to be further optimized and analyzed, although the Zn<sup>2+</sup> ion storage capacity of VO<sub>2</sub> has been improved. How are Zn<sup>2+</sup> ion transported in the coating layer and at the interface between the coating and VO<sub>2</sub>? How to balance the excellent ion diffusion and e<sup>-</sup> transport in the coating layer? In addition, issues such as the thickness of the coating also require detailed attention and control. And, it is also possible to focus on how this coating can be combined with other optimization strategies to achieve synergies of different modification methods.

### 4.3. Built-In Electric Field Strategy

The sluggish ion/electron transport kinetics is one of the major challenges in VO<sub>2</sub> storage of Zn<sup>2+</sup> ion, which will cause the dissatisfactory rate performance and power density, etc. Interestingly, breaking the original evenly distributed electronic structure in VO<sub>2</sub> to optimize the reactive microenvironment in which Zn<sup>2+</sup> ions are stored in VO<sub>2</sub> is an effective means to accelerate the kinetics process.

The built-in electric field can be critical to the reaction kinetics, and it is also very beneficial for maintaining the structural stability of VO<sub>2</sub>. In general, there is a potential difference caused by the interface plan due to energy band differences when different materials come into contact, which will facilitate the directional movement of electrons until an almost negligible difference in Fermi energy levels.<sup>[36]</sup> The charge distribution gradient will exist between the rich electron area and poor electron area for the formation of built-in electric field, which could help to increase the reaction activity and increase the reaction rate.<sup>[37]</sup>

Usually, the construction of heterojunction interface and the introduction of defects such as the common vacancy and heteroatom doping will break the original charge balance of VO<sub>2</sub> and induce charge redistribution, thus forming an internal electric field in VO<sub>2</sub>.

#### 4.3.1. Oxygen Vacancy Defects Strategy

The vacancy defects by removing of specific atoms had been applied in the field of rechargeable batteries and catalysis.<sup>[38]</sup> In this case for AVZB, the interaction between zinc ions and the oxygen of VO<sub>2</sub> will be reduced for promoting the diffusion process of Zn<sup>2+</sup> ion. Importantly, the oxygen vacancy acts as

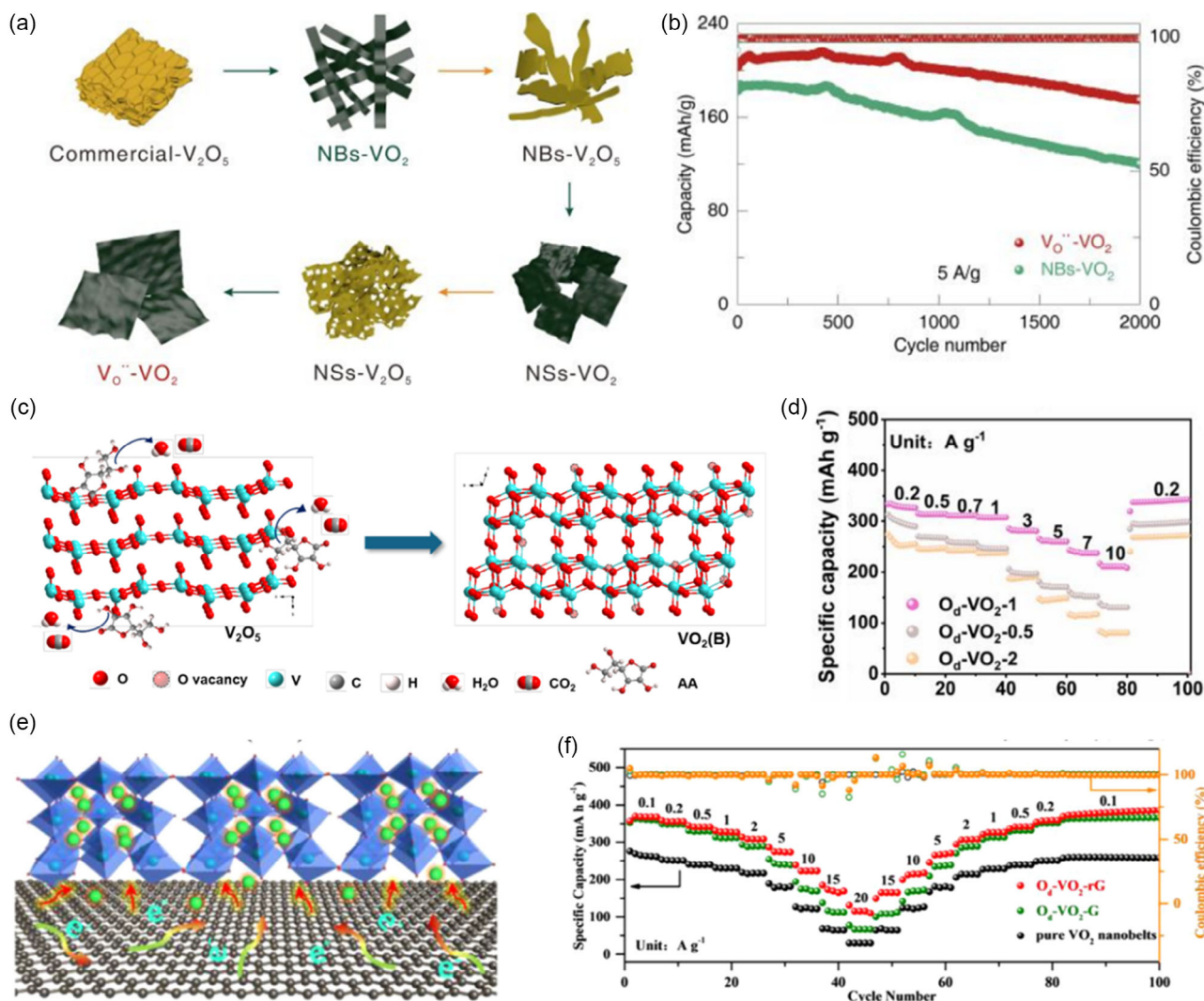


**Figure 9.** a,b) The preparation process of  $V_{O''}$ - $VO_2(B)$  and the cycling performance at  $5 \text{ A g}^{-1}$ . Reproduced with permission.<sup>[40]</sup> Copyright 2022, The American Chemical Society. c,d) The preparation process of  $V_{O'''}$ - $VO_2(B)$  and the comparison of rate performance with different concentrations of oxygen-defects. Reproduced with permission.<sup>[41]</sup> Copyright 2023, Wiley-VCH. e) Schematic illustration for the electron and ion transfer at the interface and f) the rate performance. Reproduced with permission.<sup>[42]</sup> Copyright 2020, Elsevier.

electron donor to produce large charge-accumulation area at an atomic level and this uneven charge redistribution could format the local electrical field to anchor easily foreign ions via the Coulombic electrostatic interactions to accelerate the charge exchange process.<sup>[39]</sup> Li et al.<sup>[40]</sup> introduced oxygen vacancies  $V_{O''}$  into  $VO_2(B)$  by the repeated phase change and induced larger layer spacing and jumping site for charge transport (Figure 9a,b). The narrow bandgap and lower ion diffusion energy barriers in  $V_{O''}$ - $VO_2(B)$  were also demonstrated according to density functional theory (DFT) result. As a result, the  $V_{O''}$ - $VO_2(B)$  retained a more specific capacity of  $175 \text{ mA h g}^{-1}$  (85% of retention rate) than pure  $VO_2$  of  $120 \text{ mA h g}^{-1}$  (65% of retention rate) at high current density of  $5 \text{ A g}^{-1}$  after 2000 cycles. However,  $VO_2(B)$  with oxygen defect was prepared by repeated phase change engineering, which greatly increased the time and cost of the experiment. Thus, we recently prepared

the oxygen-deficiency  $VO_{2-x}(B)$  by the  $\text{NaBH}_4$  solution reaction at room temperature.<sup>[10c]</sup> And, the oxygen defect was demonstrated with the help of XPS, positron annihilation lifetime spectroscopy, electron paramagnetic resonance (EPR) spectra, and UV-vis diffuse reflectance spectra. This  $VO_{2-x}(B)$  also showed a high-specific capacity, faster  $\text{Zn}^{2+}$  ion diffusion coefficient, and higher proportional of pseudocapacitance contribution than that of  $VO_2$ , thus the former displayed the superior ability to store  $\text{Zn}^{2+}$  ion even increasing loading of active material to  $4 \text{ mg cm}^{-2}$ .

After all, oxygen vacancy is to remove a part of oxygen atoms, which may produce an impact on the overall crystal structure, thus the possibly differential  $\text{Zn}^{2+}$  ion storage performance will be appeared based on the different concentrations of oxygen vacancies. Si et al. introduced in situ the engineering of oxygen vacancies on  $VO_2$  by adding different ratios of ascorbic acid (Figure 9c).<sup>[41]</sup> Demonstrating that the optimum oxygen vacancy

concentration will achieve excellent performances of higher capacity and fast kinetics, but the excessive vacancy can cause the opposite effects due to the reduced active sites and possibly unstable structure (Figure 9d). Moreover, Luo et al.<sup>[42]</sup> (Figure 9e,f) and Huang et al.<sup>[43]</sup> demonstrated the synergistic modification of conductive rGO and oxygen defect in the composite of VO<sub>2</sub>(B)@rGO, which can produce more stable structure and abundant active sites for achieving superior Zn<sup>2+</sup> ion storage.

Oxygen-defect in VO<sub>2</sub> cathode had improved the cycling performance via the achievement of increased reaction activity, extra sites, and built-in electron field. However, how to reasonably regulate the oxygen vacancy concentration to meet the excellent electrochemical performance while maintaining the structural stability still needs to be further explored. In addition, oxygen defect preparation methods with low cost, high safety, and factory scale should also be emphasized.

#### 4.3.2. Heteroatom-Doping Strategy

As another common defect strategy, heteroatom doping has received increasing attention to reconstruct and optimize the

intrinsic electron configuration after break the balance charge distribution for the formation of the local electrical field. This may be an internal solution for the issues of poor conductivity and insufficient active sites in VO<sub>2</sub> to enhance kinetics and rate performance. Cai et al. selected Ni<sup>2+</sup> ions as dopant to replace V<sup>4+</sup> ions due to the similar ion radius (0.055 nm vs 0.058 nm) for the easy substitution into VO<sub>2</sub>(B).<sup>[44]</sup> The electronic reorganization appeared in the (Ni)VO<sub>2</sub> after the introduction of Ni<sup>2+</sup> ion which can accumulate electrons at Ni sites and attract the electron to the surrounding O atom to change the V<sup>4+</sup> into V<sup>5+</sup> based on the DFT results (Figure 10a,b). Thus, the Zn/(Ni)VO<sub>2</sub> battery obtained superior cycling stability, lower charge transfer impedance, and high capacitive contribution ratios for enhanced kinetics (Table 1, Figure 10c). Similarly, Li et al.<sup>[45]</sup> and Gao et al.<sup>[46]</sup> demonstrated that the W-doped VO<sub>2</sub> via the replaction of W<sup>6+</sup> to V<sup>4+</sup> had rapid diffusion kinetics, enhanced structural stability, and improved conductivity and the latter also explored the suitable dopant content of 1.5 at%. Furthermore, the heteroatom (Cr, Mo, and W)-doped VO<sub>2</sub>(B) cathode was prepared under the substitution way in our groups to explore the modification-mechanism of ion doping for providing the guidance for

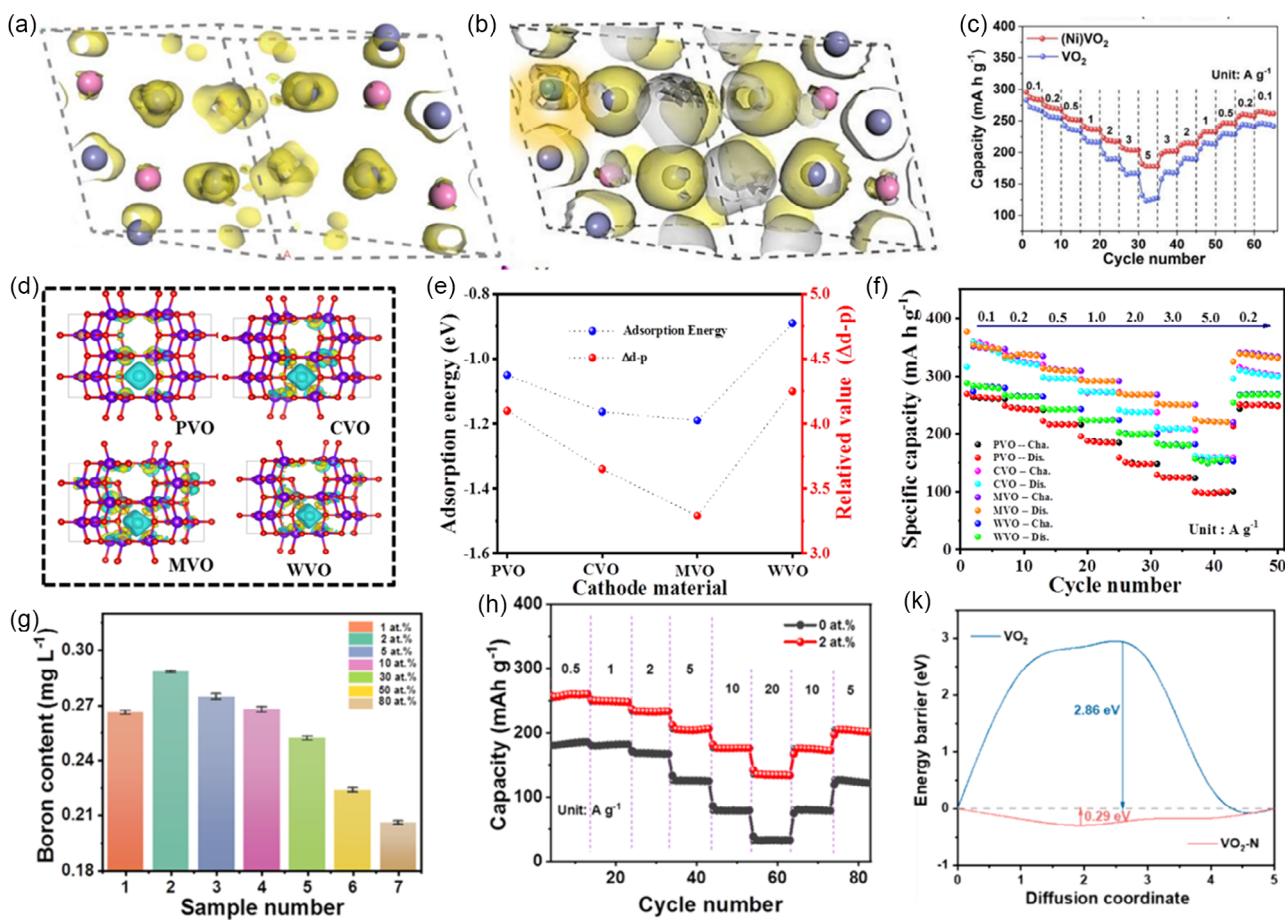


**Figure 10.** a,b) The electron density difference between (Ni)VO<sub>2</sub> and pure VO<sub>2</sub>. c) The rate performance. (a–c) Reproduced with permission.<sup>[44]</sup> Copyright 2020, The American Chemical Society. d,e) The differential charge densities diagrams and correlation between  $\Delta d-p$  and the Zn<sup>2+</sup> ion adsorption energy in P-, C-, M-, and WVO f) the rate performance. (d–f) Reproduced with permission.<sup>[47]</sup> Copyright 2023, Elsevier. g) The boron content in VO<sub>2</sub> and the comparison of performance between the 2 at% boron addition and pure VO<sub>2</sub>. g,h) Reproduced with permission.<sup>[48]</sup> Copyright 2022, Wiley-VCH. i) The Zn<sup>2+</sup> ion diffusion energy barrier in VO<sub>2</sub> and N-VO<sub>2</sub> cathode. Reproduced with permission.<sup>[49]</sup> Copyright 2023, Elsevier.

the design strategy of VO<sub>2</sub>.<sup>[47]</sup> The d-p energy difference between the O 2p orbit and d orbit of dopants could provide suggestion for screening the dopant atom according to the combination of experiment and DFT results, which will further influence the reactivity of vanadium atom and select the Mo atom with the smallest d-p value as the better dopants for AVZB (Figure 10d–f).

However, the transition metal element usually has big atomic weight, which may be not beneficial for theoretical specific capacity. Moreover, this metal ion always replaces V site instead of the O atom due to their similar properties and thus still existing the electrostatic interactions between the Zn<sup>2+</sup> and O<sup>2-</sup> ion, although the possible oxygen defects to maintain the charge balance when doped for VO<sub>2</sub>. Therefore, in addition to metal cation-doping strategies, the anion dopants with smaller ion radii and light atomic weight also recently were introduced into VO<sub>2</sub> to occupy O<sup>2-</sup> ion sites. This type of anion-doping still could induce uneven electron distribution in VO<sub>2</sub> and optimize simultaneously the lattice stability or layer spacing for enhanced Zn<sup>2+</sup> ion storage ability for AVZB. Wang et al.<sup>[48]</sup> designed interstitial B-doped VO<sub>2</sub>(B) cathode due to the advantages in light atomic weight of 11 g mol<sup>-1</sup> and smaller ion radius of 0.027 nm as well as selected the 2 at% B the suitable dopant content (Figure 10g,h). Not surprisingly, this B-doped VO<sub>2</sub> obtained a substantially increased specific capacity and enhanced kinetic process, such as 142.2 mA h g<sup>-1</sup> at 20 A g<sup>-1</sup> and excellent capacity retention of 133.3 mA h g<sup>-1</sup> at 5 A g<sup>-1</sup> after 1000 cycles. Coincidentally, the N-doped VO<sub>2</sub> also displayed the similarly improved ability to store Zn<sup>2+</sup> benefiting from the expanded lattice, improved electronic properties, and reduced Zn<sup>2+</sup> ion diffusion energy barrier (Figure 10i).<sup>[49]</sup>

Moreover, in the heteroatom doping strategy, in addition to the above substitution doping mode, the introduced foreign heteroatoms may also be located in a larger size tunnel of VO<sub>2</sub>, similar to the Zn<sup>2+</sup> ions inserted into the host materials during the discharge process. In this case, those guest heteroatoms usually play the pillar effect for maintaining the stability of VO<sub>2</sub> crystal structure,<sup>[50]</sup> also the electron structure could be reconstructed for the balanced charge to improve electrical conductivity and ion diffusion kinetics. Liu et al.<sup>[51]</sup> introduced Na<sup>+</sup> with a large ion radius and H<sup>+</sup> into VO<sub>2</sub> as supporting pillars to prevent the structure from collapse and accelerate the charge/electron transfer process. And, another H-doped VO<sub>2</sub>(B) and alkali metal ion of K<sup>+</sup> with large radius are also selected as a dopant to improve the electrochemical properties of VO<sub>2</sub>.<sup>[52]</sup>

Moreover, the polyvalent metal ions with more positive charge could comparatively form stronger chemical bonds with O to protect structural stability. Deng et al. and Li et al., all selected the Mn<sup>2+</sup> ion as pillars to dope it into the tunnel in VO<sub>2</sub> for modifying its electronic structure, which achieved enhanced electrical conductivity and improved redox activity for superior performance.<sup>[16a,19a]</sup> Furthermore, under the extra help of polyvinylpyrrolidone (PVP), Liu et al. demonstrated that the synergistic effect of Mn<sup>2+</sup> preintercalation with modified electronic structure and PVP-modified nanostructure to provide large specific surface area for boosting the reactive sites and kinetics for enhancing the cycling stability in AVZB.<sup>[53]</sup>

However, compared to the abovementioned doping mode of internal substitution, this type of interstitially doping may occupy the active sites and block diffusion channel as well as induce the

electrostatic repulsive force between them and Zn<sup>2+</sup> ion due to their the positive charge properties. Thus, the proper doping concentration should be carefully designed and controlled, and the doping site and the influence mechanism on zinc ion transport need to be further studied.

#### 4.3.3. Heterojunction Interface Chemistry Strategy

Optimization of local electronic structure can also be achieved usually by combining different materials to construct heterostructures, which will separate the electrons and holes within the materials due to the different Fermi energy of each component.<sup>[54]</sup> Thus, the built-in electric fields will appear at the interface which will act as active sites and accelerator to adsorb Zn<sup>2+</sup> ion and also facilitate the ion/electron transport kinetics process, respectively.

In our groups, we recently synthesized heterostructured VO<sub>2</sub>/rGO and VO<sub>2</sub>@CC composites based on rGO and carbon cloth, respectively (Figure 11a,b).<sup>[55]</sup> A combination of DFT results and corresponding experiments results, the higher specific capacity, longer cycling life, and faster ion/e<sup>-</sup> transmission process had been achieved in above two heterostructured-VO<sub>2</sub> cathode. This mainly was attributed to the existing of internal electric field after the electron flows from carbon to VO<sub>2</sub> for quicker and increased Zn<sup>2+</sup> ion storage preferentially at the interface. Also, N-doped VO<sub>2</sub>/C stranded on the surface of carbon nanotube fiber with the assistance of polypyrrole had obtained the heterostructures to enhance Zn<sup>2+</sup> ion storage ability and accelerated ion/e-kinetics.<sup>[10b]</sup> Additionally, the new-fashioned MXene with the advantages mentioned in last section assisted VO<sub>2</sub>@MXene composite with heterojunction to enhance Zn<sup>2+</sup> ion diffusion ability in VO<sub>2</sub>(B) and increase the capacity, such as V<sub>2</sub>C-, Ti<sub>3</sub>C<sub>2</sub>-, and Ta<sub>4</sub>C<sub>3</sub>-based MXene (Figure 11c–e).<sup>[56]</sup>

However, the above proposed carbon-based substrate material usually could only adsorb little number of Zn<sup>2+</sup> ions and only play role to construct the heterostructure which will reduce the energy density and other performance. And while the MXene only can be used after etching MAX phase particles with dangerous acid/alkali in the majority situation or it can store Zn<sup>2+</sup> ion in some specific condition (such as specific electrolyte).<sup>[57]</sup> In this case, if the substrate-material can store Zn<sup>2+</sup> ion under mild and safe conditions, it will be necessary in addition to playing the role of building heterojunctions interface. Tong et al.<sup>[58]</sup> proposed MOF-derived heterostructured C@VO<sub>2</sub>@V<sub>2</sub>O<sub>5</sub> as cathode for AVZB to obtain superior performance, such as faster diffusion coefficients, high reversible capacity, and capacity maintained (Table 1), where the abundant active sites and rapid intercalation kinetics of Zn<sup>2+</sup> ions can be achieved due to the existing of the heterojunction interface at the two-phase of VO<sub>2</sub> and V<sub>2</sub>O<sub>5</sub> (Figure 11f,g). Moreover, the V<sub>2</sub>O<sub>5</sub> with advantages of considerable theoretical specific capacity (589 mA h g<sup>-1</sup>) and suitable layer structure has been applied as promising cathode for AZMB, which can act as host materials to store Zn<sup>2+</sup> ions for increased capacity.<sup>[59]</sup> The surfaced carbon layer also could further enhance the electrical conductivity of VO<sub>2</sub>@V<sub>2</sub>O<sub>5</sub> composite.

There is only some positive effect at the two-phase interface in this strategy which may have a limited role for ion/electron



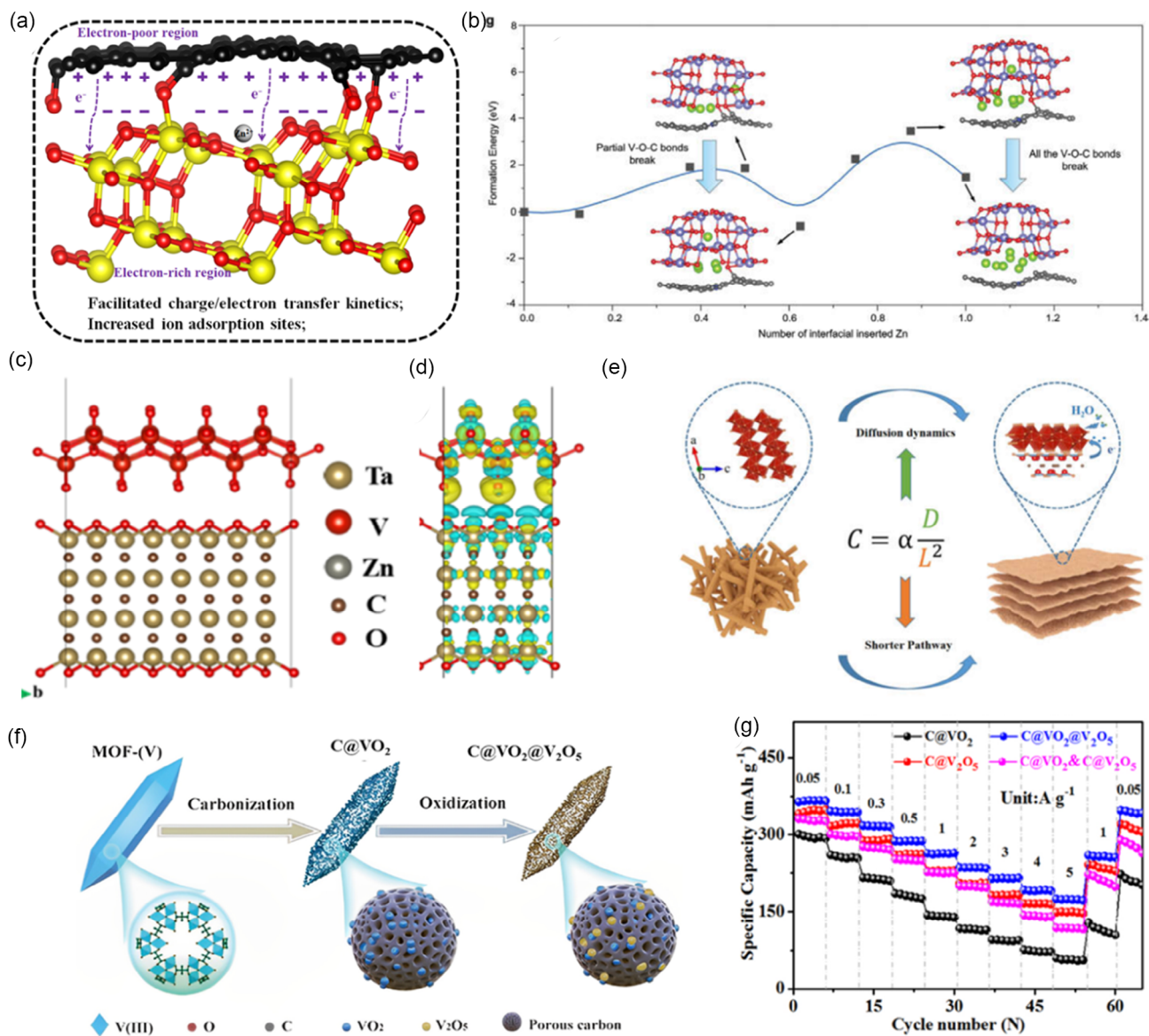


**Figure 11.** a) Schematic illustration of the built-in electrical field. Reproduced with permission.<sup>[55a]</sup> Copyright 2022, Springer Nature. b) Formation energy evolution during Zn<sup>2+</sup> ion insertion into the interface. Reproduced with permission.<sup>[55b]</sup> Copyright 2021, Wiley-VCH. c,d) The schematic diagram of VO<sub>2</sub>(B)@Ta<sub>4</sub>C<sub>3</sub> and corresponding charge density differences of VO<sub>2</sub>(B)@Ta<sub>4</sub>C<sub>3</sub>. Reproduced with permission.<sup>[56b]</sup> Copyright 2023, The Royal Society of Chemistry. e) Schematic diagram of rate performance improvement for VO<sub>2</sub>@V<sub>2</sub>C. Reproduced with permission.<sup>[56a]</sup> Copyright 2022, The Royal Society of Chemistry. f) Schematic illustration of the synthesis process of heterostructured C@VO<sub>2</sub>@V<sub>2</sub>O<sub>5</sub> and g) rate performance. Reproduced with permission.<sup>[58]</sup> Copyright 2023, Elsevier.

transport in the deeper structure of VO<sub>2</sub> so we need to consider and combine this strategy with other modification methods to exert synergies effect.

#### 4.4. Design of Optimized Electrolyte for AVZB

The electrolyte usually plays an indispensable role in connecting the circuit and providing and conducting charge ions in rechargeable battery, thus the modification of the electrolyte is also of great significance for the development of AVZB. At present, it is believed that there are the following major issues in AVZB from the perspective of electrolyte: the high-reactive water

will attack the zinc anode and the VO<sub>2</sub> cathode, and the existing of OER and HER could limit the electrochemical working voltage window within the 2.0 V.<sup>[60]</sup> Currently, there are following common principles in designing a suitable electrolyte for aqueous metal ion battery, such as reduce the activity of H<sub>2</sub>O or the content of water, regulate the solvation structure of Zn<sup>2+</sup> ions, and format the protective coating layer, etc.<sup>[1c,61]</sup> This optimized electrolyte usually could be prepared for AVZB by the addition of extra ions or molecules, specific contenting Zn<sup>2+</sup> ion electrolyte, and construction of the quasi-solid electrolyte.

The electrolyte with different anion group could provide the effect with noticeable difference in the VO<sub>2</sub> storage process of

Zn<sup>2+</sup> ions. Usually, compared to the common ZnSO<sub>4</sub>, the Zn(CF<sub>3</sub>SO<sub>3</sub>)<sub>2</sub> and Zn(TFSI)<sub>2</sub> electrolytes could reduce the number of water molecules surrounding Zn<sup>2+</sup> ion to weaken the solvation effect based on the large bulky anions effect.<sup>[62]</sup> However, the high price become the major issue in future application, thus, the new type of electrolyte should be paid more attention. Wang et al.<sup>[63]</sup> prepared three low-cost electrolyte of Zn(ClO<sub>4</sub>)<sub>2</sub>, Zn(CH<sub>3</sub>COO)<sub>2</sub>, and ZnSO<sub>4</sub> and selected the Zn(ClO<sub>4</sub>)<sub>2</sub> as the promising electrolyte for AVZB. The Zn(ClO<sub>4</sub>)<sub>2</sub> electrolyte first obtained the reversible Zn/Zn<sup>2+</sup> reaction process over the 3500 h (0.5 mA cm<sup>-2</sup> at 0.5 mA h cm<sup>-2</sup>) and with the low overpotential of 50 mV (Figure 12a), which can be attributed to the thin coating layer for protecting the Zn anode and allowing the Zn deposition underneath after the reduction of ClO<sub>4</sub><sup>-</sup>. The side production of carboxyl-containing and Zn<sub>4</sub>(OH)<sub>6</sub>SO<sub>4</sub>·xH<sub>2</sub>O in the latter two electrolytes, respectively, could increase the overpotential and shorter cycling life (Figure 12b). Thus, the VO<sub>2</sub>/Zn(ClO<sub>4</sub>)<sub>2</sub>/Zn achieved a high capacity of about 150 mA h g<sup>-1</sup> at 2 A g<sup>-1</sup> after 500 cycles.

Moreover, the negative effect of H<sub>2</sub>O with high reactivity could be reduced significantly by the preparation of quasi-solid-state

electrolyte, which not only retains some advantage of aqueous electrolyte, but also suppresses the side reaction of H<sub>2</sub>O. Shi et al.<sup>[64]</sup> developed the Zn(CF<sub>3</sub>SO<sub>3</sub>)<sub>2</sub>-PVA hydrogel electrolyte and explored the Zn<sup>2+</sup> ion storage ability of VO<sub>2</sub>@multiwalled carbon nanotubes in microbattery. This battery delivers high reversible capacity and considerable energy density and power density within 0–2 V (Table 1). Worthy, it also exhibited high flexibility and high-temperature resistance due to the substantial reduction of water molecules. Subsequently, the flexible polyacrylamide-chitin nanofiber (PAM-ChNF) hydrogel electrolyte also was proposed with high performance, which notably chemically self-charged based on the redox reaction between the VO<sub>2</sub> cathode and O<sub>2</sub> in ambient conditions (Figure 12c,d).<sup>[65]</sup> However, we should balance the content of liquid water in this quasi-solid electrolyte to take into account the advantages between liquid and solid-state batteries. And, attention also should be paid to the effect of dissolved oxygen on the electrode (especially the zinc anode) when designing this type of self-rechargeable battery.

Another effective strategy applied in electrolyte modification is the targeted introduction of additives. The different addition will induce a significantly differentiated modification effect based on

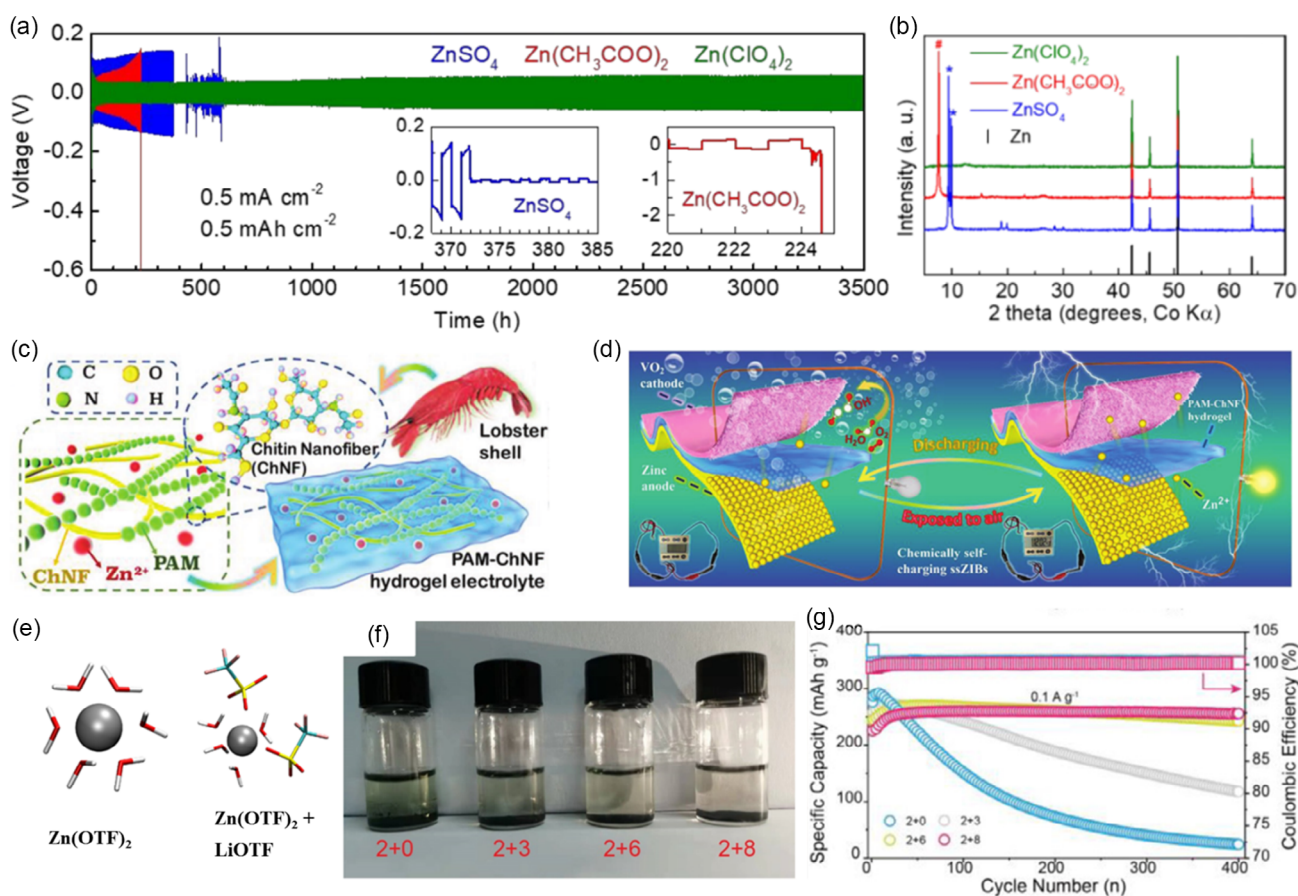


**Figure 12.** a) Zn stripping/plating behavior in Zn//Zn battery at 0.5 mA cm<sup>-2</sup> with capacity of 0.5 mA h cm<sup>-2</sup>. b) XRD of Zn anode after 50 cycles in three electrolytes. (a,b) Reproduced with permission.<sup>[63]</sup> Copyright 2019, The Royal Society of Chemistry. c,d) Schematic illustration and characterizations of PAM–ChNF hydrogel electrolyte and corresponding working mechanism of chemically self-charging in Zn//PAM–ChNF hydrogel//VO<sub>2</sub> battery. Reproduced with permission.<sup>[65]</sup> Copyright 2021, Wiley-VCH. e) Solvation structures of Zn<sup>2+</sup> ion in two electrolytes, f) cycling performance at 0.1 A g<sup>-1</sup>, and g) optical images of the VO<sub>2</sub> sample after soaking in four concentration electrolytes after 3 h. Reproduced with permission.<sup>[66]</sup> Copyright 2022, Elsevier.

the different mechanisms. Recently, a novelty type of 2M Zn(OTF)<sub>2</sub> + 8M LiOTF electrolyte has been prepared to reduce the number of free water molecules and regulate the electrolyte structure after the addition of LiOTF (Figure 12e).<sup>[66]</sup> As a result, the stable electrolyte–electrode interface formed and the cathode obtained the effectively protection by the reduction of active H<sub>2</sub>O in the tunnel and suppressed the amorphous transformation process to achieve the goal of inhibiting vanadium dissolution in AVZB (Figure 12f). Thus, the VO<sub>2</sub> achieved the capacity retention rate of 98.2% after 400 cycles at relatively low current density of 0.1 A g<sup>-1</sup>, which was rare in previous studies for mainly focusing on the cycling ability at high current density (Figure 12g). Similarly, Xu et al.<sup>[67]</sup> also reported the EDT-3Na with strong affinity with Zn<sup>2+</sup> ions optimized ZnSO<sub>4</sub> electrolyte by suppressing the formation of [Zn(H<sub>2</sub>O)<sub>6</sub>]<sup>2+</sup> to change zinc deposition behavior and suppress zinc dendrites, which enables uniform deposition on the surface of zinc anode to achieve better performance and highly reversible specific capacity in VO<sub>2</sub> side.

Although the design of the electrolyte has been paid attention by researchers, most of them are currently limited to modification measures such as the presence of additives and only focus on the performance of the electrolyte itself and the anode. However, the electrolyte acts as a pathway between the VO<sub>2</sub> cathode and zinc anode, and the influence of the newly designed electrolyte on the VO<sub>2</sub> electrode material should also be studied, such as the change of VO<sub>2</sub> structure after Zn<sup>2+</sup> ions insertion or the difference of Zn<sup>2+</sup> ions diffusion.

In conclusion, the challenge issues encountered by VO<sub>2</sub> in the process of storing zinc ions have been alleviated by the above-mentioned modification strategies, but at the same time, each modification strategy also has certain potential drawbacks and the effect and potential shortcomings of different modifications for aqueous VO<sub>2</sub>//Zn battery has been summarized in Table 2.

## 5. Summary and Outlook

In this article, based on the analysis of the structure of VO<sub>2</sub>, the energy storage mechanism of VO<sub>2</sub> as cathode material for

aqueous zinc-ion batteries was first introduced. Second, the challenges faced by VO<sub>2</sub> storage of zinc ions, such as poor conductivity and vanadium dissolution, are summarized. Finally, the modification strategies proposed to solve the above problems are summarized and analyzed in detail, such as special nanostructure engineering, composite material engineering, built-in electric field strategy, and electrolyte modification strategy. Although VO<sub>2</sub> as a kind of extremely important electrode material has shown great application prospect in aqueous zinc-ion batteries and obtained significant achievement in recent years, as far as the current development situation is concerned and there is still some considerations to be further promoted from the following aspects for the further meaningful development and industrial application.

### 5.1. Attention for the Theoretical Computational Simulation and Machine Learning

In AVZB, the detailed energy storage and modification mechanism still need to be explored well and these mysteries cannot be solved well from existing characterization techniques. The theoretical computational simulation, such as density functional theory and molecular dynamics, has received increasing attention and application in the investigation of materials, which can help obtain the properties of VO<sub>2</sub> and, electrode and zinc anode at the electron and atom level to understand the regulation mechanism of electrode materials in close to reality situations. Moreover, the current development of machine learning technology could furthermore build and design the improved VO<sub>2</sub> cathode materials and prospected aqueous Zn/VO<sub>2</sub> battery, which can greatly reduce the cost of trial and error.

### 5.2. Development of Integrated In Situ Characterization Techniques

At present, information such as the structure evolution of VO<sub>2</sub> during the Zn<sup>2+</sup> ion insertion/extraction process can only be obtained through a single in situ characterization or ex situ

**Table 2.** The mechanism, results, and potential shortcomings of different modifications for aqueous Zn/VO<sub>2</sub> battery.

Strategy	Mechanism	Result	Potential shortcoming
Design of microstructure	Promote electrolyte penetration; reduce the diffusion path length; releasing stress effect	Faster ion diffusion; increased storage site;	Aggregation issue; material dissolution; not suitable for industrial synthesis;
Composite strategy	Synergistic effect; increased the conductivity; slow material dissolution; releasing stress effect;	Promoted electronic transport; enhanced rate performance;	Unfavorable ion transport; potentially reduced active material ratio;
Built-in electric field strategy	Reconstruct the crystal and electronic structure; stronger chemical bonds; increased reaction activity;	Additional storage sites; promoted electronic/ion transport; reduced material dissolution;	Foreign ion/H <sub>2</sub> O occupy Zn <sup>2+</sup> ion diffusion/storage channels; potentially unstable structure of VO <sub>2,x</sub> ; reduce weight-specific capacity by the elements with heavy atomic mass;
Design of optimized electrolyte	Reduce the proportion and activity of water molecules;	Broaden the electrochemical window; reduced material dissolution	Increased electrolyte viscosity; potentially complex Zn <sup>2+</sup> ion storage mechanism;

characterization technology, and the latter is also faced with the impact of air atmosphere on the electrode and increased time-cost to test many batteries at specific condition. Thus, the development of integrated in situ inspection platform technology by combining multiple in situ characterizations should be paid attention to and is of great significance to the development of AVZB. This can help to capture and analyze in situ the crystal structure, apparent morphology, electronic structure, ion transport, and electrode–electrolyte interface evolution during electrochemical reactions under working conditions from atomic and molecular scales. Moreover, in situ technology also may provide some possibility to monitor the structure evolution of VO<sub>2</sub> in modified modification, which can understand and better modulation current VO<sub>2</sub> cathode.

### 5.3. Comprehensive Consideration and Optimization of VO<sub>2</sub>

It can be found that the single modification strategy focuses on the VO<sub>2</sub> cathode in most situations, which may not be conducive to the overall performance improvement and application of AVZB. Thus, we should reasonably design the high-performance VO<sub>2</sub> cathode by the synergistic effect. And, the AVZB should be evaluated under real conditions to achieve industrial-scale manufacturing.

### 5.4. Consideration of Suitable Electrolyte, Separator, and Zinc Anode

The main strategy is focused on the VO<sub>2</sub>-self and still lacks the modification electrolyte, separator, and zinc anode. Typically, the glass fiber usually as a separator with the poor mechanical properties and high price will affect further application. Thus, the separator should have the following dominant features of excellent electrolyte wetting performance, excellent thermal stability, reliable mechanical strength, low resistance and high porosity, good chemical stability, and selection of permeability. The optimization of the uniform deposition/dissolution process of zinc ions on the anode surface is also of great importance. Moreover, the electrolyte is very important in the stable operation of the battery as the part connecting VO<sub>2</sub> cathode and zinc anode, which requires the new electrolyte to be compatible with the properties of compatible electrode interface, wide electrical window, high operating voltage, good stability, and low cost, etc.

### Acknowledgements

This work was supported by the National Natural Science Foundation of China (52172233, 52172231, 51832004 and 51972259), Hainan Provincial Joint Project of Sanya Yazhou Bay Science and Technology City (2021CXLH0007), and the Natural Science Foundation of Hubei Province (2022CFA087).

### Conflict of Interest

The authors declare no conflict of interest.

### Keywords

aqueous zinc metal batteries, cathodes, modification strategies, vanadium dioxide

Received: July 15, 2023

Revised: September 3, 2023

Published online:

- [1] a) Y. Liang, Y. Yao, *Nat. Rev. Mater.* **2022**, *8*, 109; b) Y. Liang, H. Dong, D. Aurbach, Y. Yao, *Nat. Energy* **2020**, *5*, 646; c) Y. Xu, X. Zhou, Z. Chen, Y. Hou, Y. You, J. Lu, *Mater. Today* **2023**, *66*, 339.
- [2] a) X. Yu, Z. Li, X. Wu, H. Zhang, Q. Zhao, H. Liang, H. Wang, D. Chao, F. Wang, Y. Qiao, H. Zhou, S.-G. Sun, *Joule* **2023**, *7*, 1145; b) X. Guo, G. He, *J. Mater. Chem. A* **2023**, *11*, 11987; c) W. Du, E. H. Ang, Y. Yang, Y. Zhang, M. Ye, C. C. Li, *Energy Environ. Sci.* **2020**, *13*, 3330.
- [3] a) X. Jia, C. Liu, Z. G. Neale, J. Yang, G. Cao, *Chem. Rev.* **2020**, *120*, 7795; b) Y. Ding, L. Zhang, X. Wang, L. Han, W. Zhang, C. Guo, *Chinese Chem. Lett.* **2023**, *34*, 107399; c) Y. Zeng, D. Luan, X. W. Lou, *Chem* **2023**, *9*, 1118; d) Z. Xing, G. Xu, J. Han, G. Chen, B. Lu, S. Liang, J. Zhou, *Trends Chem.* **2023**, *5*, 380.
- [4] a) J. Zheng, P. Shi, C. Chen, X. Chen, Y. Gan, J. Li, J. Yao, Y. Yang, L. Lv, G. Ma, L. Tao, H. Wang, J. Zhang, L. Shen, H. Wan, H. Wang, *Sci. China Mater.* **2023**, *66*, 3113; b) T. Xiong, Y. Zhang, W. S. V. Lee, J. Xue, *Adv. Energy Mater.* **2020**, *10*, 2001769.
- [5] a) L. Ma, S. Chen, C. Long, X. Li, Y. Zhao, Z. Liu, Z. Huang, B. Dong, J. A. Zapien, C. Zhi, *Adv. Energy Mater.* **2019**, *9*, 1902446; b) Y. Tan, H. Yang, C. Miao, Y. Zhang, D. Chen, G. Li, W. Han, *Chem. Eng. J.* **2023**, *457*, 141323; c) Y. Zeng, X. F. Lu, S. L. Zhang, D. Luan, S. Li, X. W. D. Lou, *Angew. Chem. Int. Ed.* **2021**, *60*, 22189.
- [6] J. Kim, S. H. Lee, C. Park, H. S. Kim, J. H. Park, K. Y. Chung, H. Ahn, *Adv. Funct. Mater.* **2021**, *31*, 2100005.
- [7] a) L. Chen, Y. Ruan, G. Zhang, Q. Wei, Y. Jiang, T. Xiong, P. He, W. Yang, M. Yan, Q. An, L. Mai, *Chem. Mater.* **2019**, *31*, 699; b) Z. Cao, L. Wang, H. Zhang, X. Zhang, J. Liao, J. Dong, J. Shi, P. Zhuang, Y. Cao, M. Ye, J. Shen, P. M. Ajayan, *Adv. Funct. Mater.* **2020**, *30*, 2000472; c) X. Dai, F. Wan, L. Zhang, H. Cao, Z. Niu, *Energy Storage Mater.* **2019**, *17*, 143.
- [8] a) W. Zhang, C. Zuo, C. Tang, W. Tang, B. Lan, X. Fu, S. Dong, P. Luo, *Energy Technol-Ger* **2021**, *9*, 2000789; b) Y. Liu, X. Wu, *Nanomaterials* **2022**, *12*, 2794; c) W. Zhang, C. Zuo, C. Tang, W. Tang, B. Lan, X. Fu, S. Dong, P. Luo, *Energy Technol.* **2021**, *9*, 2000789; d) K. Cai, S. H. Luo, J. Feng, J. Wang, Y. Zhan, Q. Wang, Y. Zhang, X. Liu, *Chem Rec.* **2022**, *22*, e202100169; e) Y. Xu, G. Zhang, J. Liu, J. Zhang, X. Wang, X. Pu, J. Wang, C. Yan, Y. Cao, H. Yang, W. Li, X. Li, *Energy Environ. Mater.* **2023**, e12575; f) Z. Peng, Y. Li, P. Ruan, Z. He, L. Dai, S. Liu, L. Wang, S. Chan Jun, B. Lu, J. Zhou, *Coord. Chem. Rev.* **2023**, *488*, 215190; g) L. Chen, Q. An, L. Mai, *Adv. Mater. Interfaces* **2019**, *6*, 1900387; h) N. Liu, B. Li, Z. He, L. Dai, H. Wang, L. Wang, *J. Energy Chem.* **2021**, *59*, 134; i) X. Chen, H. Zhang, J.-H. Liu, Y. Gao, X. Cao, C. Zhan, Y. Wang, S. Wang, S.-L. Chou, S.-X. Dou, D. Cao, *Energy Storage Mater.* **2022**, *50*, 21.
- [9] a) P. Hu, P. Hu, T. D. Vu, M. Li, S. Wang, Y. Ke, X. Zeng, L. Mai, Y. Long, *Chem. Rev.* **2023**, *123*, 4353; b) M. Li, S. Magdassi, Y. Gao, Y. Long, *Small* **2017**, *13*, 1701147.
- [10] a) R. Li, X. Yu, X. Bian, F. Hu, *RSC Adv.* **2019**, *9*, 35117; b) J. Guo, L. Li, J. Luo, W. Gong, R. Pan, B. He, S. Xu, M. Liu, Y. Wang, B. Zhang, C. Wang, L. Wei, Q. Zhang, Q. Li, *Adv. Energy Mater.* **2022**, *12*, 2201481; c) W. Zhang, Y. Xiao, C. Zuo, W. Tang, G. Liu, S. Wang, W. Cai, S. Dong, P. Luo, *ChemSusChem* **2021**, *14*, 971.

- [11] L. Chen, Z. Yang, Y. Huang, *Nanoscale* **2019**, *11*, 13032.
- [12] L. Liu, F. Cao, T. Yao, Y. Xu, M. Zhou, B. Qu, B. Pan, C. Wu, S. Wei, Y. Xie, *New J. Chem.* **2012**, *36*, 619.
- [13] Y. Gao, J. Yin, X. Xu, Y. Cheng, *J. Mater. Chem. A* **2022**, *10*, 9773.
- [14] S. Zuo, J. Liu, W. He, S. Osman, Z. Liu, X. Xu, J. Shen, W. Jiang, J. Liu, Z. Zeng, M. Zhu, *J. Phys. Chem. Lett.* **2021**, *12*, 7076.
- [15] Z. Li, S. Ganapathy, Y. Xu, Z. Zhou, M. Sarilar, M. Wagemaker, *Adv. Energy Mater.* **2019**, *9*, 1900237.
- [16] a) F. Li, H. Sheng, H. Ma, Y. Qi, M. Shao, J. Yuan, W. Li, W. Lan, *ACS Appl. Energy Mater.* **2023**, *6*, 6201; b) M. Yan, P. He, Y. Chen, S. Wang, Q. Wei, K. Zhao, X. Xu, Q. An, Y. Shuang, Y. Shao, K. T. Mueller, L. Mai, J. Liu, J. Yang, *Adv. Mater.* **2018**, *30*, 1703725; c) D. Jia, K. Zheng, M. Song, H. Tan, A. Zhang, L. Wang, L. Yue, D. Li, C. Li, J. Liu, *Nano Res.* **2020**, *13*, 215.
- [17] W. Deng, Z. Xu, G. Li, X. Wang, *Small* **2023**, *19*, 2207754.
- [18] R. Li, L. Wang, Y. Tian, Y. Chao, X. Cui, Q. Xu, *Mater. Lett.* **2023**, *346*, 134541.
- [19] a) S. Deng, H. Li, B. Chen, Z. Xu, Y. Jiang, C. Li, W. Xiao, X. Yan, *Chem. Eng. J.* **2023**, *452*, 139115; b) Z. Tang, R. Zou, X. Chen, Z. Li, G. Lei, *J. Power Sources* **2023**, *569*, 233006; c) J. Ding, H. Gao, K. Zhao, H. Zheng, H. Zhang, L. Han, S. Wang, S. Wu, S. Fang, F. Cheng, *J. Power Sources* **2021**, *487*, 229369.
- [20] S. Fleischmann, J. B. Mitchell, R. Wang, C. Zhan, D. E. Jiang, V. Presser, V. Augustyn, *Chem. Rev.* **2020**, *120*, 6738.
- [21] V. Augustyn, P. Simon, B. Dunn, *Energy Environ. Sci.* **2014**, *7*, 1597.
- [22] N. Liu, X. Wu, L. Fan, S. Gong, Z. Guo, A. Chen, C. Zhao, Y. Mao, N. Zhang, K. Sun, *Adv. Mater.* **2020**, *32*, 1908420.
- [23] L. Zhang, L. Miao, B. Zhang, J. Wang, J. Liu, Q. Tan, H. Wan, J. Jiang, *J. Mater. Chem. A* **2020**, *8*, 1731.
- [24] J. Ding, Z. Du, L. Gu, B. Li, L. Wang, S. Wang, Y. Gong, S. Yang, *Adv. Mater.* **2018**, *30*, 1800762.
- [25] M.-X. Bai, J.-F. Gao, Z.-H. He, J.-F. Hou, L.-B. Kong, *Electroanal. Chem.* **2022**, *907*, 116039.
- [26] Y. Liu, P. Hu, H. Liu, X. Wu, C. Zhi, *Mater. Today Energy* **2020**, *17*, 100431.
- [27] L. Xie, W. Xiao, X. Shi, J. Hong, J. Cai, K. Zhang, L. Shao, Z. Sun, *Chem. Commun.* **2022**, *58*, 13807.
- [28] F. Cui, J. Zhao, D. Zhang, Y. Fang, F. Hu, K. Zhu, *Chem. Eng. J.* **2020**, *390*, 124118.
- [29] a) B. Yin, S. Zhang, K. Ke, T. Xiong, Y. Wang, B. K. D. Lim, W. S. V. Lee, Z. Wang, J. Xue, *Nanoscale* **2019**, *11*, 19723; b) T. Jin, Q. Han, L. Jiao, *Adv. Mater.* **2020**, *32*, 1806304.
- [30] X. Li, L. Yang, H. Mi, H. Li, M. Zhang, A. Abliz, F. Zhao, S. Wang, H. Li, *CrystEngComm* **2021**, *23*, 8650.
- [31] Z. Xu, X. Li, Y. Jin, Q. Dong, J. Ye, X. Zhang, Y. Qian, *Nanoscale* **2022**, *14*, 11655.
- [32] M. Yang, D. Ma, H. Mi, X. Yang, Y. Wang, L. Sun, P. Zhang, *J. Mater. Chem. A* **2021**, *9*, 8792.
- [33] M. Yang, Y. Wang, Z. Sun, H. Mi, S. Sun, D. Ma, P. Zhang, *J. Energy Chem.* **2022**, *67*, 645.
- [34] T.-T. Lv, X. Luo, G.-Q. Yuan, S.-Y. Yang, H. Pang, *Chem. Eng. J.* **2022**, *428*, 131211.
- [35] B. Shuai, C. Zhou, Y. Pi, X. Xu, *ACS Appl. Energy Mater.* **2022**, *5*, 6139.
- [36] X. Zhao, M. Liu, Y. Wang, Y. Xiong, P. Yang, J. Qin, X. Xiong, Y. Lei, *ACS Nano* **2022**, *16*, 19959.
- [37] Y. Dong, C. Yan, H. Zhao, Y. Lei, *Small Struct.* **2022**, *3*, 2100221.
- [38] a) Y. Zhang, L. Tao, C. Xie, D. Wang, Y. Zou, R. Chen, Y. Wang, C. Jia, S. Wang, *Adv. Mater.* **2020**, *32*, e1905923; b) F. Xiong, S. Tan, X. Yao, Q. An, L. Mai, *Mater. Today* **2021**, *45*, 169; c) S. Bai, N. Zhang, C. Gao, Y. Xiong, *Nano Energy* **2018**, *53*, 296.
- [39] J. Wang, J. G. Wang, X. Qin, Y. Wang, Z. You, H. Liu, M. Shao, *ACS Appl. Mater. Interfaces* **2020**, *12*, 34949.
- [40] Z. Li, Y. Ren, L. Mo, C. Liu, K. Hsu, Y. Ding, X. Zhang, X. Li, L. Hu, D. Ji, G. Cao, *ACS Nano* **2020**, *14*, 5581.
- [41] R. Si, S. Yi, H. Liu, F. Yu, W. Bao, C. Guo, J. Li, *Chem. Eur. J.* **2023**, *29*, e202300409.
- [42] H. Luo, B. Wang, C. Wang, F. Wu, F. Jin, B. Cong, Y. Ning, Y. Zhou, D. Wang, H. Liu, S. Dou, *Energy Storage Mater.* **2020**, *33*, 390.
- [43] S. Huang, S. He, H. Qin, X. Hou, *ACS Appl. Mater. Interfaces* **2021**, *13*, 44379.
- [44] Y. Cai, R. Chua, Z. Kou, H. Ren, D. Yuan, S. Huang, S. Kumar, V. Verma, P. Amonpattaratkit, M. Srinivasan, *ACS Appl. Mater. Interfaces* **2020**, *12*, 36110.
- [45] M. Li, J. Mou, L. Zhong, T. Liu, Y. Xu, W. Pan, J. Huang, G. Wang, M. Liu, *ACS Sustainable Chem. Eng.* **2021**, *9*, 14193.
- [46] F. Gao, H. Gao, K. Zhao, X. Cao, J. Ding, S. Wang, *J. Colloid Interface Sci.* **2022**, *629*, 928.
- [47] W. Zhang, J. Liu, W. Cai, M. Zhou, W. Zhong, G. Xiao, P. Luo, Y. Zhao, Q. An, *Chem. Eng. J.* **2023**, *464*, 142711.
- [48] S. Wang, H. Zhang, K. Zhao, W. Liu, N. Luo, J. Zhao, S. Wu, J. Ding, S. Fang, F. Cheng, *Carbon Energy* **2023**, *5*, e330.
- [49] X. Gu, J. Wang, X. Zhao, X. Jin, Y. Jiang, P. Dai, N. Wang, Z. Bai, M. Zhang, M. Wu, *J. Energy Chem.* **2023**, *85*, 30.
- [50] a) J. Wang, J. Wang, Y. Jiang, F. Xiong, S. Tan, F. Qiao, J. Chen, Q. An, L. Mai, *Adv. Funct. Mater.* **2022**, *32*, 2113030; b) C. Zuo, F. Chao, M. Li, Y. Dai, J. Wang, F. Xiong, Y. Jiang, Q. An, *Adv. Energy Mater.* **2023**, *13*, 2301014; c) L. Zhou, Q. Liu, Z. Zhang, K. Zhang, F. Xiong, S. Tan, Q. An, Y.-M. Kang, Z. Zhou, L. Mai, *Adv. Mater.* **2018**, *30*, 1801984; d) Z. Fan, W. He, M. Ni, P. Zhang, W. Tian, W. Zhang, L. Pan, Z. Sun, *Energy Technol.* **2020**, *9*, 200082.
- [51] Y. Liu, X. Wu, *Nano Energy* **2021**, *86*, 106124.
- [52] a) K. Guan, K. Duan, G. Yang, L. Tao, H. Zhang, H. Wan, R. Yang, J. Zhang, H. Wang, H. Wang, *Mater. Today Adv.* **2022**, *14*, 100230; b) Q. Li, X. Ye, Y. Jiang, E. H. Ang, W. Liu, Y. Feng, X. Rui, Y. Yu, *Mater. Chem. Front.* **2021**, *5*, 3132.
- [53] Y. Liu, Y. Zou, M. Guo, Z. Hui, L. Zhao, *Chem. Eng. J.* **2022**, *433*, 133528.
- [54] a) Y. Shen, Y. Jiang, Z. Yang, J. Dong, W. Yang, Q. An, L. Mai, *Adv. Sci.* **2022**, *9*, 2104504; b) X. Lu, Y. Shi, D. Tang, X. Lu, Z. Wang, N. Sakai, Y. Ebina, T. Taniguchi, R. Ma, T. Sasaki, C. Yan, *ACS Nano* **2022**, *16*, 4775.
- [55] a) P. Luo, W. Zhang, W. Cai, Z. Huang, G. Liu, C. Liu, S. Wang, F. Chen, L. Xia, Y. Zhao, S. Dong, L. Xia, *Nano Res.* **2022**, *16*, 503; b) Y. Dai, X. Liao, R. Yu, J. Li, J. Li, S. Tan, P. He, Q. An, Q. Wei, L. Chen, X. Hong, K. Zhao, Y. Ren, J. Wu, Y. Zhao, L. Mai, *Adv. Mater.* **2021**, *33*, 2100359.
- [56] a) J. Chen, B. Xiao, C. Hu, H. Chen, J. Huang, D. Yan, S. Peng, *ACS Appl. Mater. Interfaces* **2022**, *14*, 28760; b) W. Liu, H. Zong, M. Li, Z. Zeng, S. Gong, K. Yu, Z. Zhu, *ACS Appl. Mater. Interfaces* **2023**, *15*, 13554; c) W. Kou, L. Yu, Q. Wang, Y. Yang, T. Yang, H. Geng, X. Miao, B. Gao, G. Yang, *J. Power Sources* **2022**, *520*, 230872.
- [57] X. Li, M. Li, Q. Yang, G. Liang, Z. Huang, L. Ma, D. Wang, F. Mo, B. Dong, Q. Huang, C. Zhi, *Adv. Energy Mater.* **2020**, *10*, 2001791.
- [58] Y. Tong, Y. Zhao, M. Luo, S. Su, Y. Yang, Y. Zang, X. Li, L. Wang, J. Fang, *J. Alloys Compd.* **2023**, *932*, 167681.
- [59] a) W. Zhang, C. Tang, B. Lan, L. Chen, W. Tang, C. Zuo, S. Dong, Q. An, P. Luo, *J. Alloys Compd.* **2020**, *819*, 152971; b) P. Luo, W. Zhang, S. Wang, G. Liu, Y. Xiao, C. Zuo, W. Tang, X. Fu, S. Dong, *J. Alloys Compd.* **2021**, *884*, 161147; c) P. Luo, Z. Huang, G. Liu, C. Liu, P. Zhang, Y. Xiao, W. Tang, W. Zhang, H. Tang, S. Dong, *J. Alloys Compd.* **2022**, *919*, 165804.
- [60] Z. Liu, Y. Huang, Y. Huang, Q. Yang, X. Li, Z. Huang, C. Zhi, *Chem. Soc. Rev.* **2020**, *49*, 180.
- [61] H. Li, S. Guo, H. Zhou, *Energy Storage Mater.* **2023**, *56*, 227.

- [62] F. Wang, O. Borodin, T. Gao, X. Fan, W. Sun, F. Han, A. Faraone, J. A. Dura, K. Xu, C. Wang, *Nat. Mater.* **2018**, *17*, 543.
- [63] L. Wang, Y. Zhang, H. Hu, H. Y. Shi, Y. Song, D. Guo, X. X. Liu, X. Sun, *ACS Appl. Mater. Interfaces* **2019**, *11*, 42000.
- [64] J. Shi, S. Wang, X. Chen, Z. Chen, X. Du, T. Ni, Q. Wang, L. Ruan, W. Zeng, Z. Huang, *Adv. Energy Mater.* **2019**, *9*, 1901957.
- [65] C. Liu, W. Xu, C. Mei, M. Li, W. Chen, S. Hong, W. Y. Kim, S. Y. Lee, Q. Wu, *Adv. Energy Mater.* **2021**, *11*, 2003902.
- [66] S. Liu, J. He, D.-S. Liu, M. Ye, Y. Zhang, Y. Qin, C. C. Li, *Energy Storage Mater.* **2022**, *49*, 93.
- [67] W. Xu, Q. Xie, X. Chen, M. Wu, J. Zhang, Q. Ru, *Ionics* **2023**, *29*, 2783.
- [68] Z. Shi, Q. Ru, Z. Pan, M. Zheng, F. Chi-Chun Ling, L. Wei, *ChemElectroChem* **2021**, *8*, 1091.
- [69] Y. Liu, Y. Liu, X. Wu, Y. R. Cho, *ACS Appl. Mater. Interfaces* **2022**, *14*, 11654.
- [70] J.-S. Park, J. H. Jo, Y. Aniskevich, A. Bakavets, G. Ragoisha, E. Streltsov, J. Kim, S.-T. Myung, *Chem. Mater.* **2018**, *30*, 6777.
- [71] P. Liang, K. Zhu, J. Chen, Y. Rao, H. Zheng, J. Guo, Z. Kong, J. Zhang, J. Liu, K. Yan, J. Wang, *J. Power Sources* **2023**, *568*, 232945.
- [72] X. Yuan, Y. Nie, T. Zou, C. Deng, Y. Zhang, Z. Wang, J. Wang, C. Zhang, E. Ye, *ACS Appl. Energy Mater.* **2022**, *5*, 13692.
- [73] M. Zhang, T. Hu, X. Wang, P. Chang, L. Pan, Z. Jin, H. Mei, L. Cheng, L. Zhang, *Energy Storage Mater.* **2022**, *51*, 465.



**Wenwei Zhang** received his B.S. degree from Hubei University of Automotive Technology in 2018 and master's degree from Hubei University of Technology in 2021. He is currently working toward the Ph.D. degree at Wuhan University of Technology (WUT) in 2022. His current research interest focuses on the modification of electrode materials and ionic storage mechanisms for rechargeable magnesium metal battery and aqueous zinc metal battery.



**Wenhui Zhong** received her B.S. degree from Wuhan Polytechnic University and is currently working toward the master's degree from Hubei University of Technology in 2021. She focuses on the modification and ionic storage mechanisms of VO<sub>2</sub> for aqueous zinc metal battery.



**Junjun Wang** received his B.S. degree in materials science and engineering from Henan Polytechnic University in 2017. He received his master's degree at Wuhan University of Technology (WUT) in 2020. He is currently working toward a Ph.D. degree at WUT. His current research focuses on rechargeable magnesium and calcium batteries.



**Qinyou An** is professor of materials science and engineering at WUT. He received his Ph.D. degree from WUT in 2014. He carried out his postdoctoral research in the laboratory of Prof. Yan Yao at the University of Houston in 2014–2015. Currently, his research interest includes energy storage materials and devices.



**Liqiang Mai** is the chair professor of materials science and engineering at WUT, dean of the School of Materials Science and Engineering at WUT, and Fellow of the Royal Society of Chemistry. He received his Ph.D. from WUT in 2004 and carried out his postdoctoral research at Georgia Institute of Technology in 2006–2007. He worked as an advanced research scholar at Harvard University and the University of California, Berkeley. His current research interest focuses on new nanomaterials for electrochemical energy storage and micro/nanoenergy devices.